ARTICLE

Lineage tracing clarifies the cellular origin of tissue-resident macrophages in the developing heart

Kuo Liu[1,2,7]*, Hengwei Jin[2]*, Muxue Tang[2], Shaohua Zhang[2], Xueying Tian[3], Mingjun Zhang[2], Ximeng Han[2,7], Xiuxiu Liu[2], Juan Tang[2], Wenjuan Pu[2], Yan Li[2], Lingjuan He[4], Zhongzhou Yang[5], Kathy O. Lui[6], and Bin Zhou[1,2,3,7]

Tissue-resident macrophages play essential functions in the maintenance of tissue homeostasis and repair. Recently, the endocardium has been reported as a de novo hemogenic site for the contribution of hematopoietic cells, including cardiac macrophages, during embryogenesis. These observations challenge the current consensus that hematopoiesis originates from the hemogenic endothelium within the yolk sac and dorsal aorta. Whether the developing endocardium has such a hemogenic potential requires further investigation. Here, we generated new genetic tools to trace endocardial cells and reassessed their potential contribution to hematopoietic cells in the developing heart. Fate-mapping analyses revealed that the endocardium contributed minimally to cardiac macrophages and circulating blood cells. Instead, cardiac macrophages were mainly derived from the endothelium during primitive/transient definitive (yolk sac) and definitive (dorsal aorta) hematopoiesis. Our findings refute the concept of endocardial hematopoiesis, suggesting that the developing endocardium gives rise minimally to hematopoietic cells, including cardiac macrophages.

Introduction

The establishment of an early circulatory system is vital for embryogenesis. Among the circulating blood cells, tissue-resident macrophages of the heart are not only essential for cardiac healing after injury, but are also involved in heart development, supporting coronary angiogenesis and electrical conduction (Epelman et al., 2014a; Hulsmans et al., 2017; Lavine et al., 2014; Leid et al., 2016; Lorchner et al., 2015; Nahrendorf et al., 2007). Additionally, macrophages provide critical signals and secrete numerous soluble factors to promote the formation of new myocardium after injury during neonatal heart regeneration (Aurora et al., 2014). Unraveling the developmental origins of cardiac macrophages would also provide valuable information to advance our understanding of cardiac remodeling during homeostasis and inflammation. However, the origins of cardiac macrophages remain controversial.

The mainstream view holds that cardiac macrophages, along with other hematopoietic cells, are mainly derived from endothelial-to-hematopoietic transition (EHT) during primitive and definitive hematopoiesis in the developing mouse embryo (Boisset et al., 2010; Dzierzak and Speck, 2008; Epelman et al., 2014a; Epelman et al., 2014b; Shalaby et al., 1997). There are three waves of hematopoiesis during development. The first primitive wave arises from the blood island of the yolk sac (YS) at around embryonic day 7.5 (E7.5) and produces early primitive erythromyeloid progenitors (EMPs), contributing to YS macrophages and microglia. Shortly after the onset of primitive hematopoiesis, a transient definitive wave starts in the hemogenic endothelium (HE) of YS that produces late c-Myb[+] EMPs between E8.0 and E8.25. Transient definitive hematopoiesis can give rise to YS macrophages or multiple lineages after migration to the fetal liver through circulation at E8.5–E9.5. The primitive and transient definitive hematopoiesis of the YS region are heterogeneous (Hoeffel et al., 2015). After E8.5, the third wave of definitive hematopoiesis occurs at the para-aortic splanchnopleura and aorta-gonad-mesonephros (AGM), where hematopoietic stem and progenitor cells are generated to colonize the

[1]School of Life Science, Hangzhou Institute for Advanced Study, University of Chinese Academy of Sciences, Hangzhou, China;   [2]State Key Laboratory of Cell Biology, Shanghai Institute of Biochemistry and Cell Biology, Center for Excellence in Molecular Cell Science, University of Chinese Academy of Sciences, Chinese Academy of Sciences, Shanghai, China;   [3]Key Laboratory of Regenerative Medicine of Ministry of Education, Department of Developmental & Regenerative Biology, College of Life Science and Technology, Jinan University, Guangzhou, China;   [4]School of Life Sciences, Westlake University, Hangzhou, Zhejiang, China;   [5]State Key Laboratory of Pharmaceutical Biotechnology, Department of Cardiology, Nanjing Drum Tower Hospital, The Affiliated Hospital of Nanjing University Medical School and Ministry of Education Key Laboratory of Model Animal for Disease Study, Model Animal Research Center, Nanjing Biomedical Research Institute, Nanjing University, Nanjing, China;   [6]Department of Chemical Pathology, Li Ka Shing Institute of Health Sciences, The Chinese University of Hong Kong, Prince of Wales Hospital, Shatin, Hong Kong SAR, China;   [7]School of Life Science and Technology, ShanghaiTech University, Shanghai, China.

*K. Liu and H. Jin contributed equally to this paper.   Correspondence to Bin Zhou: zhoubin@sibs.ac.cn.

fetal liver at E11.5–E12.5, and resident macrophages are also developed after E11.5 that can subsequently migrate to the developing heart (Epelman et al., 2014b; Ginhoux and Guilliams, 2016; Gomez Perdiguero et al., 2015; Hoeffel et al., 2015; Medvinsky and Dzierzak, 1996). Therefore, hematopoietic stem and progenitor cells and all blood cell lineages specifically originate from HE. Identification of new regions containing HE will reshape our current concept of hematopoiesis and provide valuable information to study tissue homeostasis and inflammation (Grainger and Traver, 2019).

The heart tube is a special vessel-like structure that is formed after fusion of the cardiac crescent at ~E7.5 (Abu-Issa and Kirby, 2007; Deruiter et al., 1992). The initiation of heartbeat and blood flow is established from stage 5 to 8 (E8.0–E8.5) in mice. The primitive endocardial tube is formed at ~E8.25, and the heart is connected to the dorsal aorta (DA), co-occurring with primitive hematopoiesis (Ji et al., 2003). The hematopoietic progenitor–derived cells can then circulate through the embryo, including the heart (Ji et al., 2003). Previous reports suggested that the heart tube shares a similar genetic program with HE of the DA (Nakano et al., 2013). However, there is a lack of convincing genetic evidence to demonstrate the hemogenic potential of the endocardium. Whether the embryonic heart tube is indeed a de novo hemogenic site along with the YS and AGM remains unclear.

Recent studies have suggested that the endocardium contributes to transient definitive hematopoiesis in the developing heart (Grainger and Traver, 2019; Nakano et al., 2013; Shigeta et al., 2019; Zamir et al., 2017). Specifically, Nkx2.5+ endocardium-derived definitive EMPs emerge at ~E9.5 that could enter the peripheral circulation during embryogenesis (Nakano et al., 2013). Furthermore, by using the Nfatc1-Cre genetic tracing tool, it has been found that ~58% of macrophages in the endocardial cushion are derived from the Nfatc1-Cre–labeled endocardium (Shigeta et al., 2019). Genetic ablation of these macrophages results in severe valve malformation, indicating that the hemogenic activity of the endocardium and its differentiated macrophages are functionally indispensable for valve remodeling in the developing heart (Shigeta et al., 2019). Nevertheless, success in fate-mapping experiments requires cell-specific expression of gene promoters that drive the Cre recombinase. Importantly, Nkx2.5 is not a specific marker, as Nkx2.5+ cardiovascular progenitors give rise to not only the endocardium but also endothelial cells of the YS and AGM region (Zamir et al., 2017). Likewise, whether the Nfatc1-Cre tool used in the previous study (Shigeta et al., 2019) specifically labels the endocardium needs further examination. More specific lineage-tracing tools that map the cell fate of endocardium-derived cells are imperatively needed, therefore, to reassess the hemogenic potential of the developing endocardium.

In this study, we show that Nfatc1 is not a specific gene marker for targeting the endocardium. Using more specific tools to trace the cell fate of endocardium-derived cells, we demonstrate that the developing endocardium is not hemogenic and contributes minimally to cardiac macrophages and blood cells in the circulation. We further show that cardiac macrophages are mainly derived from the HE of YS and AGM through EHT during primitive, transient definitive, and definitive hematopoiesis.

Results
Intramyocardial macrophages are developed in close proximity to the endocardium

Through sectional immunostaining, we showed that cardiac macrophages first emerged at ~E10.5 and were expanded from E10.5 to E14.5 (Fig. 1 A). To understand their anatomic locations, we used the epicardium, the outermost mesothelial cell layer of the heart, and the endocardium, the innermost endothelial cell layer lining the trabecular myocardium and valves, as landmarks. We generated a Npr3-ZsGreen knock-in line (Fig. 1 B) to label the endocardium through natriuretic peptide receptor C (Npr3), a new marker identified in a previous study (Zhang et al., 2016a). To characterize the Npr3-ZsGreen line, we first stained E12.5 heart sections for ZsGreen, PLVAP (endocardium-specific marker), and VE-cad (pan-endothelial cell marker) and found that 96.43 ± 0.42% of Plvap+VE-cad+ endocardial cells were efficiently labeled by Npr3-ZsGreen (Fig. 1, C and D), confirming the specificity and efficiency of Npr3-ZsGreen in marking the endocardium. We then collected hearts for macrophage lineage analysis at the growth phase from E12.5 to E15.5 (Fig. 1 C). Immunostaining for ZsGreen and F4/80 on Npr3-ZsGreen heart sections showed that cardiac-resident macrophages were mainly localized in three areas of the developing heart: sub-epicardium, intramyocardium, and cushion/valves. The sub-epicardial macrophages could be readily discerned but were rarely found during these developmental stages. For intramyocardial macrophages, quantification of the distance between F4/80+ macrophages and ZsGreen+ endocardial cells showed that >96% of trabecular macrophages were found within 20 μm from the endocardium (Fig. 1, E and F). Regarding macrophages of the valves, by immunostaining for F4/80 and ERG, a nuclear marker of endothelial cells, we showed that >80% of them were localized within 20 μm from the endocardium in atrioventricular valves (AVs; including mitral and tricuspid valves) and semilunar valves (including aortic and pulmonary valves [Ao/PVs]) (Fig. 1, G and H). Collectively, these data show that intramyocardial and valve macrophages were distributed in close proximity to the endocardium during heart development (Fig. 1 F).

Nfatc1-based lineage tracing is not endocardium specific

The endocardium has multipotency for giving rise to various cell types of the heart including coronary endothelial cells, coronary smooth muscle cells, fibroblasts, pericytes, and adipocytes (Chen et al., 2016; de Lange et al., 2004; Liu et al., 2018; Zhang et al., 2016b). The proximal distribution of cardiac macrophages near the endocardium may suggest that the endocardium could also contribute to cardiac macrophages. In fact, by using the Nfatc1-Cre tool (Wu et al., 2012), it has been recently reported that cardiac macrophages of the cushion or valves are mainly derived from the Nfatc1-Cre–labeled endocardium (Shigeta et al., 2019). However, a subset of endothelial cells of YS and AGM are also labeled by Nfatc1-Cre (Shigeta et al., 2019), which could confound the interpretation of the fate-mapping data. To directly verify this, we used three different Nfatc1 knock-in tools, including Nfatc1-ires-Cre, Nfatc1-2A-Dre, and Nfatc1-2A-CreER (Zhang et al., 2017; Zhang et al., 2016a; Zhang et al., 2016b), to reassess the endocardial contribution of Nfatc1-derived cells to embryonic hematopoiesis.
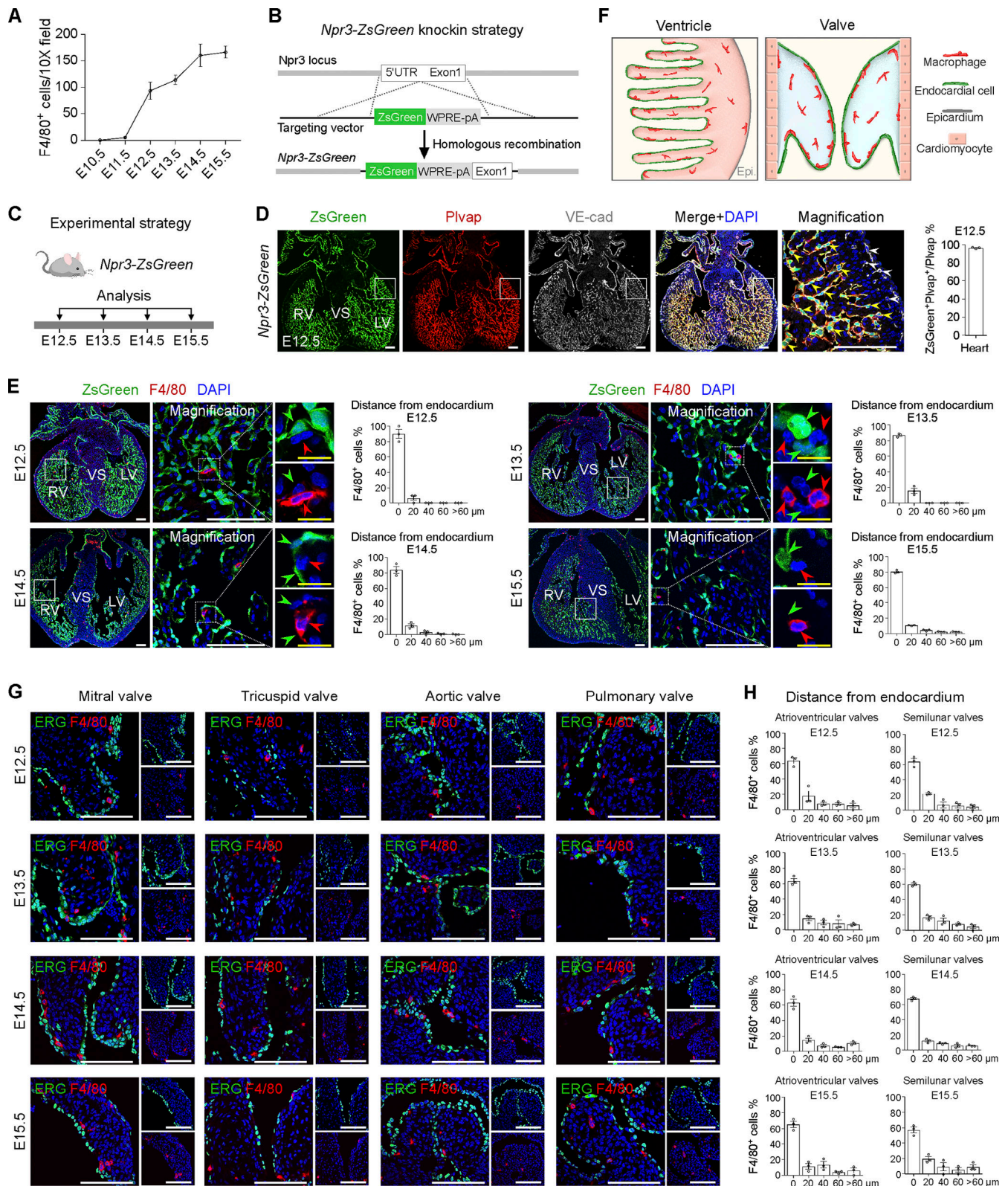
Figure 1. **Intramyocardial and valve macrophages are located close to endocardium. (A)** Quantification of the number of F4/80[+] macrophages per 10× field from E10.5 to E15.5. Data are presented as mean ± SEM; *n* = 7 mice per group. **(B)** Schematic showing knock-in strategy for generation of *Npr3-ZsGreen* mouse by homologous recombination. **(C)** Schematic showing the time points for tissue analysis using *Npr3-ZsGreen* mice. **(D)** Immunostaining for ZsGreen, Plvap, and Ve-cad on E12.5 heart sections of *Npr3-ZsGreen* mouse. Quantification of the percentage of ZsGreen[+]Plvap[+] endocardium is shown on the right. Data are presented as mean ± SEM; *n* = 3 mice per group. **(E)** Immunostaining for ZsGreen and F4/80 on heart sections of E12.5–E15.5 *Npr3-ZsGreen* mice. Red arrowheads, F4/80[+] macrophages; green arrowheads, ZsGreen^{+} endocardial cells. Quantification of the percentage of macrophages with different distances

Liu et al.
Cellular origin of cardiac macrophages

Journal of Cell Biology   3 of 19
https://doi.org/10.1083/jcb.202108093

from endocardium is shown on the right. 0 µm, the macrophage is in contact with the endocardial cell. Data are presented as mean ± SEM; *n* = 3 mice per group. **(F)** Cartoon image showing the distribution of macrophages in heart ventricle and valve. Most macrophages are close to ventricular and valvular endocardium. **(G)** Immunostaining for ERG and F4/80 on E12.5–E15.5 heart sections showing that valve macrophages are close to valvular endocardium. **(H)** Quantification of the percentage of valve macrophages with different distances from the valvular endocardium. Data are presented as mean ± SEM; *n* = 3 mice per group. LV, left ventricle; RV, right ventricle; VS, ventricular septum. Scale bars, white, 100 µm; yellow, 20 µm.

We first used the Cre recombinase–based tracing tool, *Nfatc1-ires-Cre*, to generate *Nfatc1-ires-Cre;R26-tdTomato* reporter mice by crossing with *Rosa26-loxP-Stop-loxP-tdTomato* (*R26-tdTomato*). We collected E15.5 hearts from the reporter mice for analysis (Fig. 2 A). Immunostaining on heart sections for tdTomato (tdT) and F4/80 showed that tdT[+]F4/80[+] macrophages were found in almost all regions of the developing heart, including subepicardium, compaction myocardium, trabecular myocardium, ventricular septum, atrium, AV, and semilunar valves (Fig. 2 B). Quantification of the percentage of tdT[+]F4/80[+] macrophages showed that 60.90 ± 2.50% of cardiac macrophages were labeled by *Nfatc1-ires-Cre*–based tracing (Fig. 2 C). Flow cytometric analysis further showed that *Nfatc1-ires-Cre*–labeled cells contributed to 51.92 ± 4.31% of CD45^{+}F4/80^{+} macrophages in the developing heart (Figs. 2 D and S1 A), consistent with the previous report (Shigeta et al., 2019). Furthermore, 50.50 ± 2.60% of CD45^{+} cells were labeled by tdT (Figs. 2 E and S1 B), suggesting that Nfatc1-labeled cells could contribute to circulating white blood cells.

Likewise, we used the Dre recombinase–based fate-mapping tool, *Nfatc1-2A-Dre*, to examine endocardial contribution to macrophages. The working principle of the Dre-rox recombination system is similar to that of the Cre-loxP system (He et al., 2017). We crossed *Nfatc1-2A-Dre* with *Rosa26-rox-Stop-rox-tdTomato* (*R26-RSR-tdTomato*) to generate the *Nfatc1-2A-Dre;R26-RSR-tdTomato* reporter mice and collected E15.5 hearts from these mice for analysis (Fig. 2 J). Immunostaining for tdT and F4/80 on E15.5 heart sections showed that tdT[+]F4/80[+] macrophages were detected in almost all regions of the developing heart, including subepicardium, compaction myocardium, trabecular myocardium, ventricular septum, AV, and semilunar valves (Fig. 2, J and K). Quantification of the percentage of tdT[+]F4/80[+] macrophages showed that 43.57 ± 4.03% of cardiac macrophages expressed tdT (Fig. 2 K). Flow cytometric analysis further showed that 29.07 ± 2.10% of CD45^{+}F4/80^{+} cardiac macrophages and 23.18 ± 1.92% of CD45^{+} cells of the blood were labeled by tdT, suggesting that *Nfatc1-2A-Dre*–labeled cells contributed to cardiac macrophages and circulating blood cells (Fig. 2 L).

However, the *Nfatc1* gene is not expressed specifically by the endocardium but also by other endothelial cell subsets. Previous studies have revealed the hemogenic activity of endocardium to be at ~E9.5–E11.5, which happens at the same time as endocardium-to-mesenchyme transition (Nakano et al., 2013). We therefore used three independent Nfatc1 knock-in tools (*Nfatc1-ires-Cre*, *Nfatc1-2A-Dre*, and *Nfatc1-2A-CreER*) to examine the expression of Nfatc1 in the developing endothelium. Whole-mount epifluorescence views of E9.5 *Nfatc1-ires-Cre;R26-tdTomato* showed tdT[+] signals in the heart, DA, and YS regions (Fig. 2 F). Immunostaining for tdT and endothelial cell marker platelet endothelial cell adhesion molecule (PECAM) on embryonic

sections showed that 14.79 ± 1.52% and 17.27 ± 1.17% of endothelial cells of YS and DA were labeled by tdT, respectively, which are known as the HE locations responsible for hematopoiesis (Fig. 2, G and H). Therefore, our results indicated that the cell types that were labeled by Nfatc1-based tracing such as the endothelium of DA and YS could have been overlooked in the previous work (Shigeta et al., 2019). Because Nfatc1-derived macrophages were first identified in the heart at E9.5, and subsequently in the circulation at E10.5 (Shigeta et al., 2019), we attempted to recapitulate this finding by performing immunostaining for tdT and CD45 or Ter-119 on E9.5 embryonic sections of *Nfatc1-ires-Cre;R26-tdTomato* mice. Notably, CD45^{+} tdT^{+} and Ter-119^{+}tdT^{+} blood cells were detected in other embryonic regions, in addition to the heart (Fig. 2 I). We then collected E9.5 samples of *Nfatc1-2A-Dre;R26-RSR-tdTomato* to examine whether *Nfatc1-2A-Dre* could target the HE of YS and DA. Whole-mount epifluorescence and sectional immunostaining analysis of E9.5 *Nfatc1-2A-Dre;R26-RSR-tdTomato* mice showed that 10.53 ± 0.95% and 15.20 ± 1.93% of endothelial cells of YS and DA, respectively, were labeled by tdT (Fig. 2, M and N). Immunostaining for tdT and CD45 or Ter-119 detected tdT^{+}CD45^{+} hematopoietic cells and tdT^{+}Ter-119^{+} erythrocytes on E9.5 embryonic sections (Fig. 2 O). To eliminate the influence from endocardial hematopoiesis, we removed the heart before collecting the circulating blood cells for analysis. Our data showed that 17.56 ± 1.62% and 15.26 ± 1.73% of CD45^{+} cells in the embryonic circulation and YS, respectively, were tdT^{+} (Fig. 2 P), suggesting that Nfatc1-derived cells were detected in the circulation at E9.5. Collectively, our data based on *Nfatc1-2A-Dre*–mediated tracing showed that *Nfatc1* was not a specific gene marker for targeting the endocardium.

Furthermore, we used inducible *Nfatc1-2A-CreER;R26-tdTomato* reporter mice for temporal analysis on Nfatc1 expression in the developing endothelium. We treated mice with tamoxifen (Tam) at E7.5 and collected embryos at E9.5 (Fig. 2 Q). Similarly, whole-mount epifluorescence microscopy showed that tdT[+] signals were seen in the heart, DA, somatic vessel, and YS regions (Fig. 2 R). Immunostaining for tdT and PECAM on embryonic sections showed that the endocardium was efficiently labeled by tdT (Fig. 2, T and U). Moreover, 45.71 ± 2.36% and 32.04 ± 3.75% of endothelial cells of YS and DA were labeled by tdT, respectively (Fig. 2, S–U). Here, we detected CD45^{+}tdT^{+} blood cells not only in the heart, but also a substantial number of CD45^{+}tdT^{+} cells in other embryonic regions, such as YS and somatic vessels (Fig. 2, V–X). Of note, Tam treatment at later stages (e.g., E12 or E12.5) showed reduced Nfatc1-lineage–labeled macrophages compared with treatment at earlier stages (e.g., E7.5 or E9.5; Fig. S2). These data suggest that lineage tracing based on *Nfatc1* also marked endothelial cells of YS and AGM and white blood cells in the circulation. Given the known hemogenic nature of endothelial cells in YS and AGM, we speculated that
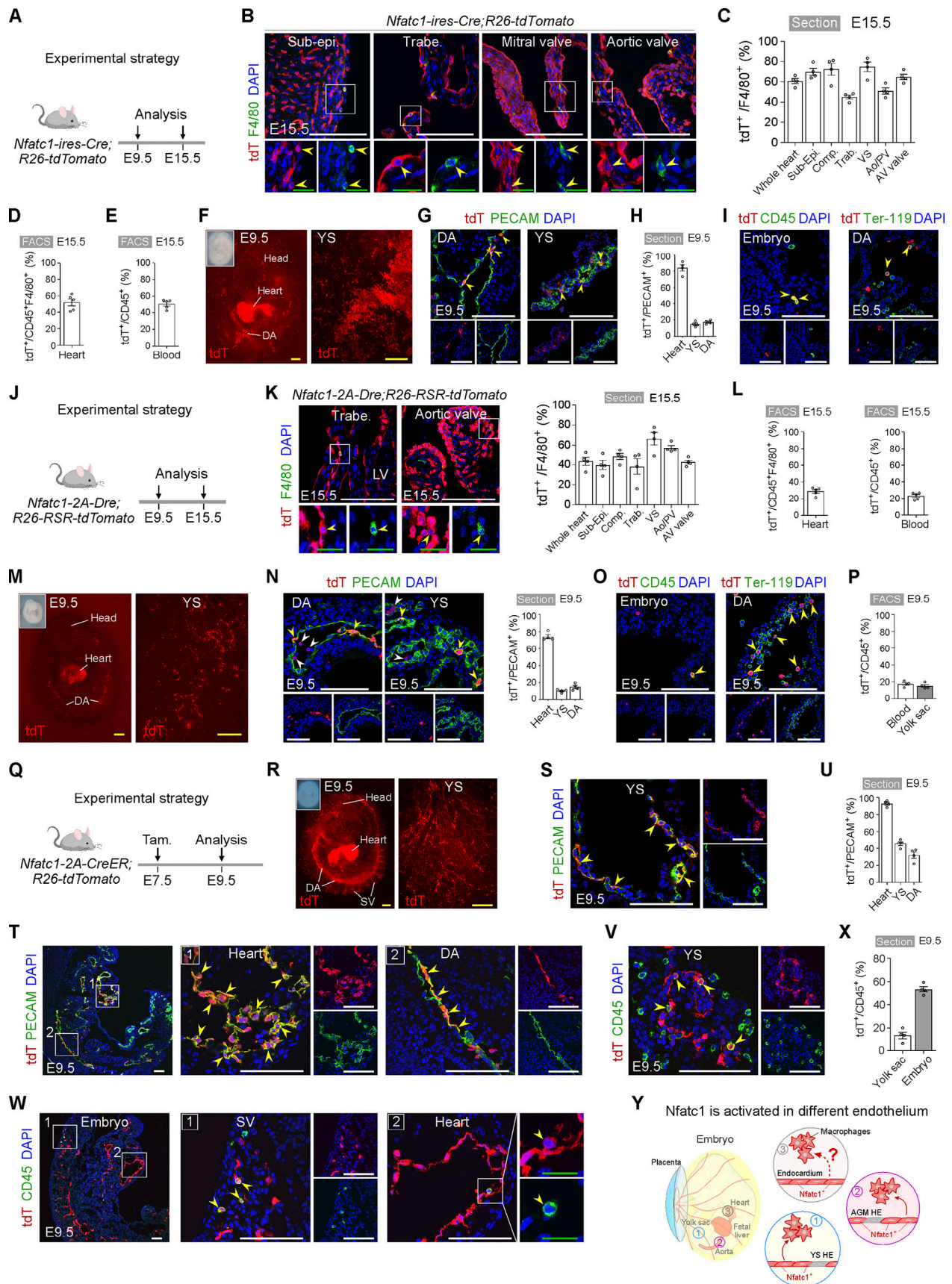
Figure 2. **Nfatc1 is expressed in endothelial cells of YS and AGM in addition to endocardium. (A)** Schematic showing the time points for tissue analysis using *Nfatc1-ires-Cre;R26-tdTomato* mice. **(B)** Immunostaining for tdT and F4/80 on E15.5 *Nfatc1-ires-Cre;R26-tdTomato* heart sections. Yellow arrowheads,

tdT⁺F4/80⁺ macrophages. **(C)** Quantification of the percentage of F4/80⁺ macrophages expressing tdT. Data are presented as mean ± SEM; *n* = 4 mice per group. **(D and E)** Flow cytometric analysis of CD45⁺F4/80⁺ macrophages of heart (D) and CD45⁺ immune cells of blood (E) expressing tdT. Data are presented as mean ± SEM; *n* = 5 mice per group. **(F)** Whole-mount bright-field and epifluorescence views of E9.5 *Nfatc1-ires-Cre;R26-tdTomato* embryo and YS. **(G)** Immunostaining for tdT and PECAM on embryonic and YS sections. Yellow arrowheads, tdT⁺PECAM⁺ endothelial cells. **(H)** Quantification of the percentage of PECAM⁺ endothelial cells expressing tdT. Data are presented as mean ± SEM; *n* = 4 mice per group. **(I)** Immunostaining for tdT and CD45 or Ter-119 on embryonic sections. Yellow arrowheads, tdT⁺CD45⁺ immune cells or tdT⁺Ter-119⁺ cells. **(J)** Schematic showing the time points for tissue analysis using *Nfatc1-2A-Dre;R26-RSR-tdTomato* mice. **(K)** Immunostaining for tdT and F4/80 on E15.5 *Nfatc1-2A-Dre;R26-RSR-tdTomato* heart sections (left). Yellow arrowheads, tdT⁺F4/80⁺ macrophages. Quantification of the percentage of F4/80⁺ macrophages expressing tdT (right). Data are presented as mean ± SEM; *n* = 4 mice per group. **(L)** Flow cytometric analysis of CD45⁺F4/80⁺ macrophages of heart (left) and CD45⁺ immune cells of blood (right) expressing tdT. Data are presented as mean ± SEM; *n* = 5 mice per group. **(M)** Whole-mount bright-field and epifluorescence views of E9.5 *Nfatc1-2A-Dre;R26-RSR-tdTomato* embryo and YS. **(N)** Immunostaining for tdT and PECAM on embryonic and YS sections (left). Yellow arrowheads, tdT⁺PECAM⁺ endothelial cells. Quantification of the percentage of PECAM⁺ endothelial cells expressing tdT (right). Data are presented as mean ± SEM; *n* = 4 mice per group. **(O)** Immunostaining for tdT and CD45 (left) or Ter-119 (right) on E9.5 *Nfatc1-2A-Dre;R26-RSR-tdTomato* tissue sections. Yellow arrowheads, tdT⁺CD45⁺ immune cells or tdT⁺Ter-119⁺ blood cells. **(P)** Flow cytometric quantification of CD45⁺ immune cells of the embryo (removal of heart) and YS expressing tdT. Data are presented as mean ± SEM; *n* = 4 mice per group. **(Q)** Schematic showing the experimental design. **(R)** Whole-mount bright-field and epifluorescence views of E9.5 *Nfatc1-2A-CreER;R26-tdTomato* embryo and YS. **(S and T)** Immunostaining for tdT and PECAM on YS (S) and embryonic (T) sections. Yellow arrowheads, tdT⁺PECAM⁺ endothelial cells. **(U)** Quantification of the percentage of PECAM⁺ endothelial cells expressing tdT. Data are presented as mean ± SEM; *n* = 4 mice per group. **(V and W)** Immunostaining for tdT and CD45 on YS (V) and embryonic (W) sections. Yellow arrowheads, tdT⁺CD45⁺ immune cells. **(X)** Quantification of the percentage of CD45⁺ cells expressing tdT. Data are presented as mean ± SEM; *n* = 4 mice per group. **(Y)** Cartoon image showing Nfatc1-labeled multitype endothelium that potentially contributes to cardiac macrophages. Comp, compaction; LV, left ventricle; RV, right ventricle; Sub-Epi, subepicardium; SV, somatic vessel; Trab, trabeculae; VS, ventricular septum. Scale bars, white, 100 µm; green, 20 µm; yellow, 1 mm.

lineage tracing through *Nfatc1* could have labeled the HE and various endothelial cell subsets in addition to the endocardium (Fig. 2 Y). Therefore, Nfatc1-based tracing was not endocardial specific.

Nfatc1 gene is autonomously expressed in macrophages and monocytes

The *Nfatc1* gene plays essential roles in regulating immune responses, especially in T cell activation (Zhou et al., 2002). The above data showed that *Nfatc1-ires-Cre*–labeled cells contributed to ∼50% CD45⁺ cells of the circulating blood (Fig. 2 E). Next, we performed flow cytometric analysis to determine which cell types of the circulating blood were marked by *Nfatc1-ires-Cre;R26-tdTomato* at E15.5. We found that *Nfatc1-ires-Cre* labeled 26.68 ± 1.62% of monocytes, 24.52 ± 0.90% of neutrophils, 13.59 ± 2.02% of T cells, 21.30 ± 0.89% of B cells, 36.26 ± 2.79% of macrophages, and 0.02 ± 0.00% of erythrocytes (Fig. 3, A–C). To test whether macrophages expressed the *Nfatc1* gene, we isolated cardiac and peritoneal macrophages and performed reverse transcription quantitative PCR (RT-qPCR) analysis (Fig. 3 D). We showed that both the cardiac and peritoneal macrophages autonomously expressed the *Nfatc1* gene (Fig. 3 E). To further test whether the Nfatc1-based tracing tool could label the Nfatc1⁺ macrophages, we performed Tam treatment in *Nfatc1-2A-CreER;R26-tdTomato* mice at E17.5, during which hematopoiesis of YS and DA has ended, and collected the heart and circulating blood at E18.5 for analysis (Fig. 3 F). Immunostaining for tdT and F4/80 on heart sections showed that 0.99 ± 0.58% of macrophages were labeled by tdT over this 1-d time frame (Fig. 3, F–I). However, because the recombination efficiency of *Nfatc1-2A-CreER;R26-tdTomato* mice was ∼30% (data not shown) using this Tam treatment strategy, the number of labeled *Nfatc1⁺* macrophages could be at least three times underestimated within this period. Considering that the *Nfatc1-ires-Cre* is constitutively active, its labeled Nfatc1⁺ cardiac macrophages could have accumulated from E10.5 when cardiac macrophages emerged at E15.5. Moreover, flow cytometric analysis of the circulating blood of *Nfatc1-2A-CreER;R26-tdTomato* mice at E18.5 showed that

5.94 ± 1.00% of circulating macrophages and 5.45 ± 0.61% of monocytes were labeled by tdT (Fig. 3, J and K). This 1-d temporal labeling data suggested that *Nfatc1* was also expressed in a subset of circulating macrophages and monocytes. Therefore, the Nfatc1⁺ cardiac macrophages labeled by *Nfatc1-ires-Cre* could directly account for the labeled macrophages in the developing heart.

Nfatc1⁺ endocardium does not have hematopoietic potential ex vivo

Runx1 is an important regulator expressed by the HE to control activation of hematopoietic gene expression (North et al., 2002). To test whether these Nfatc1⁺ endocardial cells express the hemogenic endothelial cell marker Runx1, we performed coimmunostaining for VE-cad, Runx1, and tdT on E9.5 *Nfatc1-ires-Cre;R26-tdTomato* embryonic sections (Fig. 4 A). The results showed that the tdT⁺ VE-cad⁺ Runx1⁺ endothelial cells were detected in YS, but not in the outflow tract (OFT)/heart region (Fig. 4, B and C). Furthermore, we observed many tdT⁺ Runx1⁺VE-cad⁻ cells in the vascular lumen and heart chambers, and most of them expressed CD45, suggesting that these committed blood progenitor cells may originate from other Runx1⁺ HE through blood circulation (Fig. 4, D and E). The absence of endocardial expression of the hemogenic endothelial marker Runx1 in vivo suggested that the endocardium was less likely to have hematopoietic activity.

Because current genetic tools do not enable us to exclusively trace Nfatc1⁺ endocardial cells in vivo, we then performed ex vivo hematopoietic colony-forming assays to reassess the hematopoietic potential of the endocardium. We used E8.0 embryos for ex vivo experiments because the circulatory system has not yet been fully established at this moment. Briefly, the YS, caudal half, head, and heart regions of E8.0 *Nfatc1-ires-Cre;R26-tdTomato* embryos were dissected and precultured on OP9 stromal cells for 4 d and transferred to methylcellulose medium for 10 d according to the protocols described by Nakano et al. (2013; Fig. 5 A). The YS and caudal half were included as the positive control groups, and the head was used as the negative control group. Our ex vivo results showed that the tdT⁺
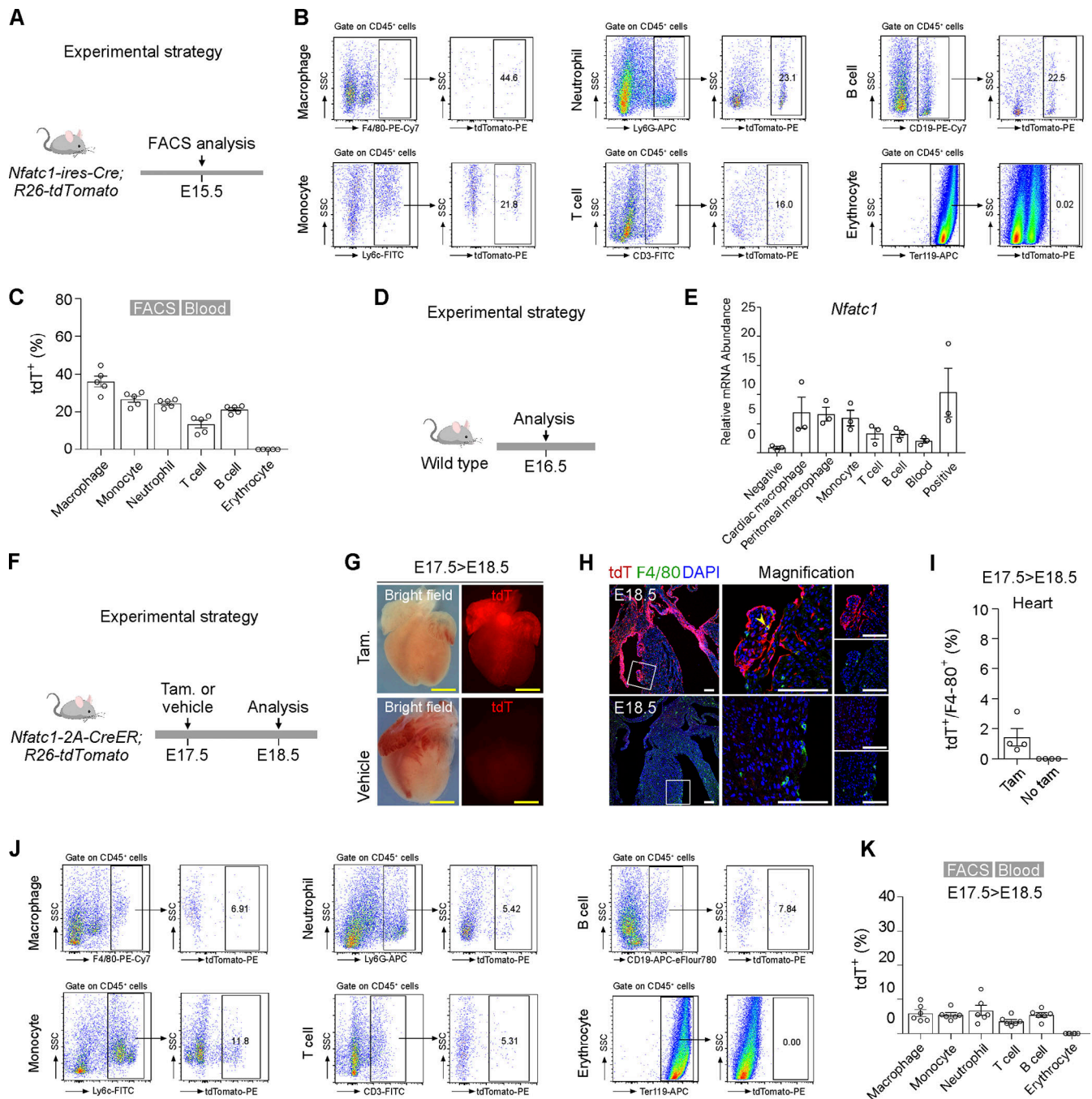
Liu et al.
Cellular origin of cardiac macrophages

Journal of Cell Biology   6 of 19
https://doi.org/10.1083/jcb.202108093

Figure 3. **Nfatc1 gene is expressed in white blood cells. (A)** Schematic showing the experimental design. The blood of E15.5 *Nfatc1-ires-Cre;R26-tdTomato* mice was isolated for flow cytometric analysis. **(B and C)** Flow cytometric analysis (B) and quantification (C) of the percentage of circulating macrophages, monocytes, neutrophils, T cells, B cells, and erythrocytes that express tdT of E15.5 *Nfatc1-ires-Cre;R26-tdTomato* mice. Data are presented as mean ± SEM; n = 5 mice per group. SSC, side scatter. **(D and E)** RT-qPCR analysis of the *Nfatc1* gene expression in different cell types isolated from E16.5 wild-type mice. Cardiomyocyte was set as a negative control; endocardial cell was set as a positive control. Data are presented as mean ± SEM; n = 3 mice per group. **(F)** Schematic showing the experimental design. **(G)** Whole-mount fluorescence of E18.5 *Nfatc1-2A-CreER;R26-tdTomato* embryo after Tam or corn oil (vehicle) treatment at E17.5. **(H)** Immunostaining for tdT and F4/80 on E18.5 heart sections of *Nfatc1-2A-CreER;R26-tdTomato* mice after Tam treatment at E17.5. Yellow arrowheads, tdT+F4/80+ macrophages. **(I)** Quantification of the percentage of F4/80+ macrophages expressing tdT. Data are presented as mean ± SEM; n = 4 mice per group. **(J and K)** Flow cytometric analysis (J) and quantification (K) of tdT-labeled macrophages, monocytes, neutrophils, T cells, B cells, and erythrocytes of E18.5 circulating blood of *Nfatc1-2A-CreER;R26-tdTomato* mice after Tam treatment at E17.5. Data are presented as mean ± SEM; n = 6 mice per group. Scale bars, yellow, 1 mm; white, 100 μm.

Liu et al.
Cellular origin of cardiac macrophages

Journal of Cell Biology 7 of 19
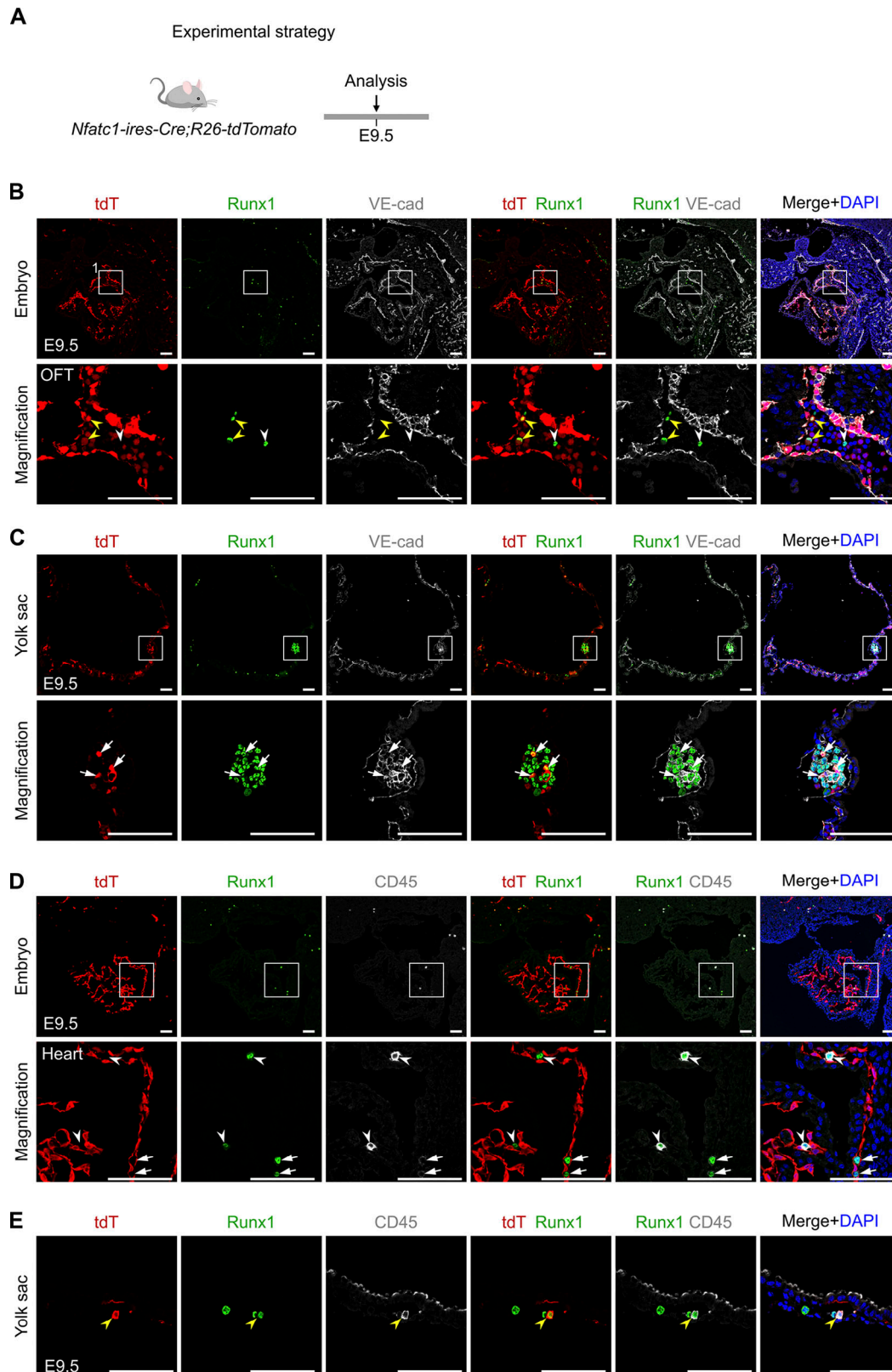https://doi.org/10.1083/jcb.202108093

Figure 4. **Nfatc1⁺ endocardium does not express the hemogenic endothelial marker Runx1. (A)** Schematic showing the experimental strategy. **(B and C)** Immunostaining for tdT, Runx1, and VE-cad on the sections of embryo (B) and YS (C) of E9.5 *Nfatc1-ires-Cre;R26-tdTomato* mice. Yellow arrowheads, tdT⁺Runx1⁺VE-cad⁻ circulating blood cells; white arrowheads, tdT⁻Runx1⁺VE-cad⁻ circulating blood cells; white arrows, tdT⁺Runx1⁺VE-cad⁺ endothelial cells. **(D and E)** Immunostaining for tdT, Runx1, and CD45 on the sections of embryo (D) and YS (E) of E9.5 *Nfatc1-ires-Cre;R26-tdTomato* mice. Yellow arrowheads, tdT⁺Runx1⁺CD45⁺ circulating blood cells; white arrowheads, tdT⁻Runx1⁺CD45⁺ circulating blood cells; white arrows, tdT⁻Runx1⁺CD45^low circulating blood cells. Scale bars, 100 µm. *n* = 5 mice per group.

macrophage colonies were generated from both the YS and caudal half groups, but neither from the head nor the heart groups (Fig. 5, B and C). Immunostaining for tdT and F4/80 or CD45 further confirmed that Nfatc1$^+$ cells contributed to macrophages in YS and AGM but not in head nor heart groups (Fig. 5, D and E). Collectively, these data supported that the Nfatc1$^+$ endocardial cells did not have hemogenic potential.

Mef2c-derived endocardium minimally contributes to cardiac macrophages and circulating blood cells

Mef2c is a secondary/anterior heart field (SHF/AHF) progenitor marker, and Mef2c-AHF-Cre–derived cells are highly restricted to the AHF of the developing heart (De Val et al., 2004). A previous genetic fate-mapping study showed that Mef2c-AHF-Cre$^+$ cells contribute to endocardial cells as well as cardiomyocytes of the right ventricle and OFT (Verzi et al., 2005). To further examine the hemogenic activity of the endocardium, we used the *Mef2c-AHF-Cre;R26-tdTomato* reporter mice to track the contribution of SHF progenitor-derived endocardium to hematopoietic cells at E10.5 and E15.5 (Fig. 6 A). Whole-mount epifluorescence microscopy of the E10.5 embryo showed that tdT$^+$ signal was only detected in the heart, but not in other regions such as AGM or YS (Fig. 6 B). Immunostaining for tdT and PECAM on E10.5 embryonic sections showed that 81.44 ± 2.08% of OFT endocardial cells and 25.7 ± 1.47% of atrial endocardial cells were tdT$^+$, whereas endothelial cells of YS and AGM were tdT$^-$ (Fig. 6, C–E). It has been previously reported that the Nkx2.5-lineage–labeled endocardium of the OFT and atrium contributes to peripheral Ter119$^+$ erythroid cells and CD45$^+$ cells at E10.5 (Nakano et al., 2013). A study from the same group further showed that the Nfatc1$^+$ endocardial cells give rise to cardiac macrophages at the embryonic stages, which persists in the adult stage (Shigeta et al., 2019). However, immunostaining for tdT, CD45, F4/80, or Ter119 on E10.5 embryonic sections of the *Mef2c-AHF-Cre;R26-tdTomato* reporter mice showed that none of these cells expressed tdT (Fig. 6, F, G, I, and J; and Fig. S3, A–C). Flow cytometric analysis also revealed that the tdT$^+$ cell population was hardly detected among CD45$^+$ or Ter-119$^+$ blood cells (Fig. 6, H and K; and Fig. S3 D). Moreover, immunostaining for tdT and F4/80 (Fig. 6 L) or CD45 (Fig. 6 M) on E15.5 heart sections also showed the absence of F4/80$^+$tdT$^+$ (Fig. 6 N) or CD45$^+$tdT$^+$ (Fig. 6 O) cells, suggesting that *Mef2c-AHF-Cre*–derived endocardium did not contribute to cardiac macrophages and blood cells. Flow cytometric analysis further confirmed that virtually no tdT$^+$ cell population was detected among F4/80$^+$ cardiac macrophages or CD45$^+$ circulating white blood cells (Fig. 6, P and Q; and Fig. S3 E). Because the genetic tdT label of endocardial cells by *Mef2c-AHF-Cre* was permanent and irreversible, the tdT$^-$ cells detected in the heart or blood were unlikely to be derived from the endocardium. These genetic fate-mapping data further demonstrated that the endocardium did not have hemogenic potential for giving rise to cardiac macrophages or circulating blood cells (Fig. 6 R).

Npr3-derived endocardium contributes minimally to cardiac macrophages and circulating blood cells

Similarly, *Npr3* is another gene marker of the endocardium, so we used the *Npr3-CreER;R26-tdTomato* reporter that targets the

endocardium to further assess its hemogenic potential with an additional marker (Zhang et al., 2016a). It has been recently reported that cardiac macrophages emerge at ~E9.5 (Shigeta et al., 2019). To target the endocardium efficiently, we induced *Npr3-CreER;R26-tdTomato* reporter mice with two doses of Tam, at E7.5 and E8.5, and collected embryos at E10.5 and E15.5, respectively, for analysis (Fig. 7 A). Whole-mount epifluorescence microscopy of E10.5 embryos showed that tdT$^+$ signals were concentrated in the heart but not in the YS region (Fig. 7 B). Immunostaining for tdT and PECAM on embryonic sections showed that 95.47 ± 0.87%, 90.52 ± 1.60%, and 55.17 ± 2.53% of endocardial cells of the atrium, ventricle, and OFT—but not of the YS region—were labeled by tdT (Fig. 7, C–E). Having established this strategy for efficiently labeling the endocardium, we determined if these labeled cells contributed to CD45$^+$ cells. However, immunostaining for tdT and CD45 or F4/80 of E10.5 embryonic sections showed that Npr3$^+$ endocardium contributed minimally to CD45$^+$ or F4/80$^+$ cells of the heart (Fig. 7 F; and Fig. S4, A–C). Immunostaining for tdT and Ter-119 showed that no Ter119$^+$ cell was labeled by tdT (Fig. 7 G). Flow cytometric analysis of E10.5 embryo and circulating blood further revealed that neither CD45$^+$ nor Ter-119$^+$ cells were tdT$^+$ (Fig. 7, H and I; and Fig. S4 D). We also collected E15.5 heart for analysis. Immunostaining for tdT, F4/80, and CD45 on E15.5 heart sections did not locate any tdT$^+$F4/80$^+$ macrophages or tdT$^+$CD45$^+$ white blood cells (Fig. 7, J and K). Flow cytometric analysis further showed the absence of tdT$^+$ population among F4/80$^+$ cardiac macrophages or CD45$^+$ circulating white blood cells, indicating that the Npr3$^+$ endocardium contributed minimally to cardiac macrophages (Fig. 7, L and M; and Fig. S4 E). Taken together, these data demonstrated that the Npr3$^+$ endocardium was not hemogenic during embryogenesis (Fig. 7 N).

Subepicardial macrophages are not derived from the epicardium

By virtue of the available genetic tools that label the endocardium, our extensive experiments did not display its hemogenic potential, even though cardiac macrophages were localized closely to the endocardium. Through sectional immunostaining, we noticed that a subset of cardiac macrophages was seen in the subepicardium. Because epicardial cells have also been considered as progenitors of the developing mouse heart (Tian et al., 2015), we used *Wt1-CreER;R26-tdTomato* reporter mice to trace the cell fate of the epicardial cells and addressed whether the epicardium could give rise to cardiac macrophages (Fig. 8 A). However, our fate-mapping analysis revealed that no F4/80$^+$ cell was labeled by tdT in these reporter mice, indicating that subepicardial macrophages were not derived from the epicardium (Fig. 8, A–D).

Cardiac macrophages originate from primitive, transient definitive, and definitive hematopoiesis

The above lineage-tracing experiments revealed that the intramyocardial and valve macrophages were not derived from the endocardium, and the subepicardial macrophages did not originate from the epicardium. Primitive hematopoiesis begins at ~E7.5 in the YS, followed by transient definitive hematopoiesis
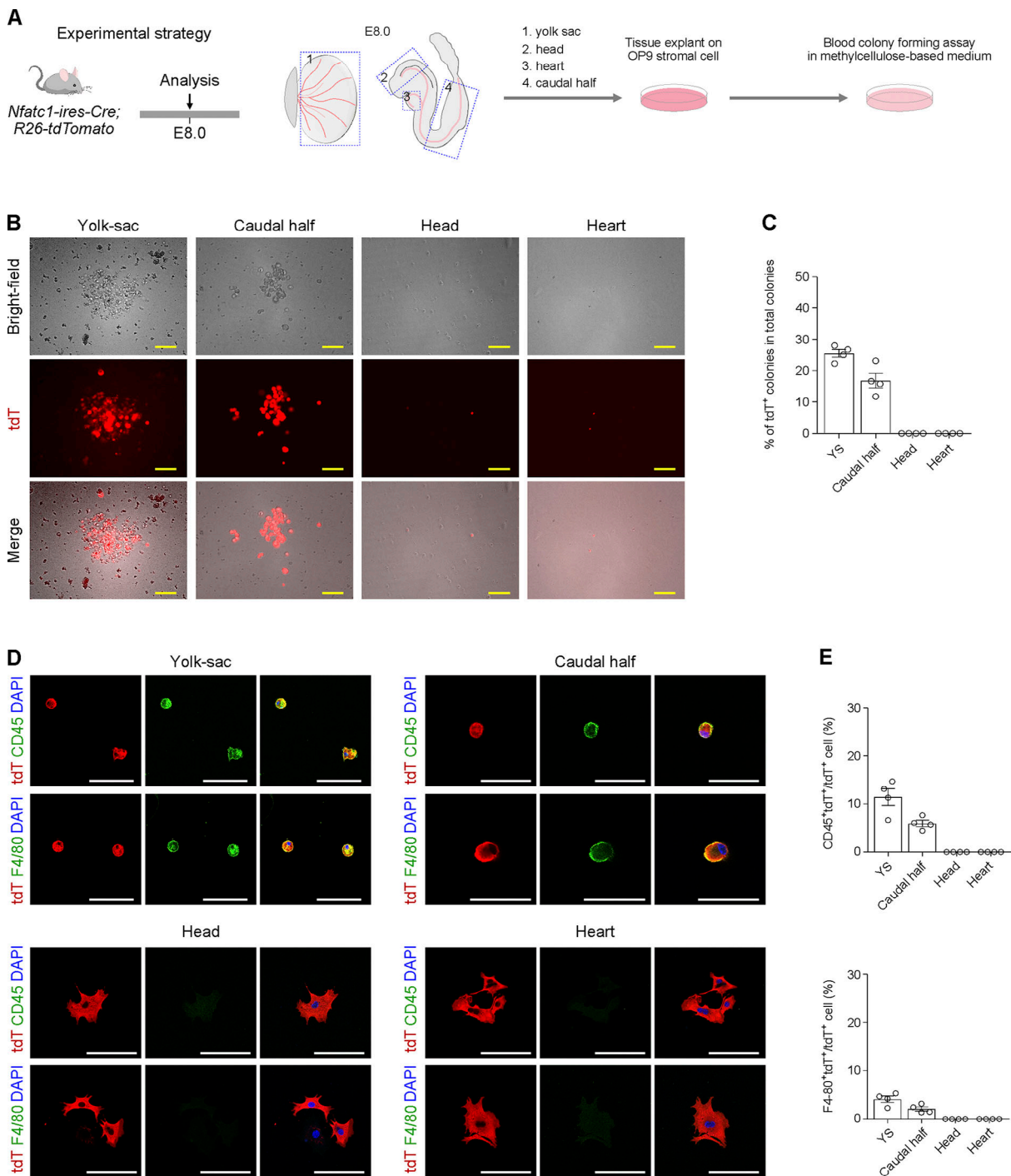
Liu et al.
Cellular origin of cardiac macrophages

Journal of Cell Biology   9 of 19
https://doi.org/10.1083/jcb.202108093

Figure 5. **Nfatc1+ endocardium does not show hematogenic properties in ex vivo hematopoietic colony-forming assays. (A)** Schematic showing the experimental design. The YS, caudal half, head, and heart of E8.0 *Nfatc1-ires-Cre;R26-tdTomato* mice were respectively dissected and precultured on OP9 stromal cells and then transferred onto methylcellulose medium for testing hematopoietic colony formation. **(B)** Whole-mount bright-field and fluorescence images of the representative macrophage colonies after culturing in methylcellulose medium for 10 d. **(C)** Quantification of the percentage of tdTomato+ colonies in ex vivo hematopoietic colony-forming assays. Data are presented as mean ± SEM; *n* = 4 mice per group. **(D)** Immunostaining for tdTomato, CD45, and F4/80 after 10 d of culture in methylcellulose medium. **(E)** Quantification of the percentage of tdT+ cells expressing CD45 or F4/80. Data are presented as mean ± SEM; *n* = 4 mice per group. Scale bars, yellow, 100 μm; white, 30 μm.

at ~E8.0 and then definitive hematopoiesis in the AGM region at ~E10.5 (Epelman et al., 2014a; Ginhoux and Guilliams, 2016; Gomez Perdiguero et al., 2015; Hoeffel et al., 2015). We therefore examined if the HE of YS and AGM gives rise to cardiac macrophages located at different regions of the developing heart during these three waves of hematopoiesis.

To examine the contribution of cardiac macrophages during EHT of primitive and transient definitive hematopoiesis, we
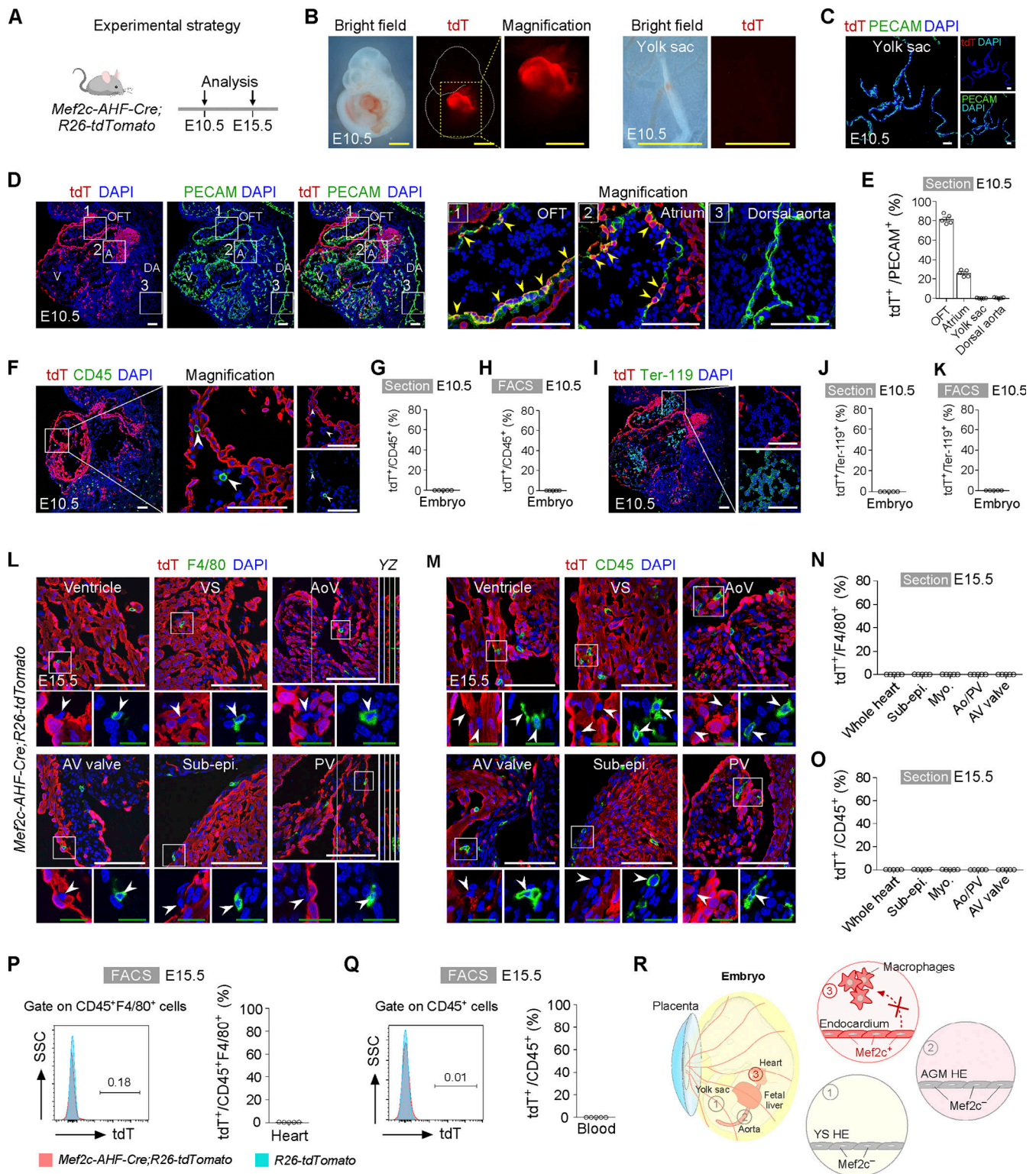
Figure 6. **Mef2c-Cre–labeled endocardium contributes minimally to heart macrophages. (A)** Schematic showing the time points for tissue analysis using *Mef2c-AHF-Cre;R26-tdTomato* mice. **(B)** Whole-mount fluorescence of E10.5 embryo and YS. **(C and D)** Immunostaining for tdT and PECAM on sections of E10.5 YS (C) and embryo (D). Yellow arrowheads, tdT⁺PECAM⁺ endocardial cells. **(E)** Quantification of the percentage of PECAM⁺ endothelial cells expressing tdT in different regions. Data are presented as mean ± SEM; *n* = 5 mice per group. **(F)** Immunostaining for tdT and CD45 on sections of E10.5 embryo. White arrowheads, tdT⁻CD45⁺ immune cells. **(G)** Quantification of the percentage of CD45⁺ cells expressing tdT. Data are presented as mean ± SEM; *n* = 5 mice per group. **(H)** Flow cytometric quantification of CD45⁺ immune cells of embryo expressing tdT. Data are presented as mean ± SEM; *n* = 5 mice per group. **(I)** Immunostaining for tdT and Ter-119 on E10.5 embryonic section. **(J)** Quantification of the percentage of Ter-119⁺ cells expressing tdT. Data are presented as mean ± SEM; *n* = 5 mice per group. **(K)** Flow cytometric quantification of Ter-119⁺ cells of embryo expressing tdT. Data are presented as mean ± SEM; *n* = 5 mice per group. **(L and M)** Immunostaining for tdT and F4/80 (L) or CD45 (M) on E15.5 heart sections. White arrowheads, tdT⁻F4/80⁺ macrophages or

generated a new *Cdh5-2A-CreER* knock-in line for targeting the HE of YS and AGM (Fig. 9 A), treated *Cdh5-2A-CreER;R26-tdTomato* reporter mice with 4-hydroxytamoxifen (4OHT) at E7.5, and performed analysis at E12.5 and E16.5 (Figs. 9 B and S5 A). Immunostaining for tdT and PECAM on E16.5 sections showed that endothelial cells of the heart and YS were efficiently labeled by tdT (98.65 ± 0.46% and 98.60 ± 0.79%, respectively; Fig. 9, B–D). Consistent with the previous report (Ginhoux et al., 2010), we also confirmed that almost all microglia (97.02 ± 0.72%) were labeled when 4OHT was given at E7.5, indicating efficient genetic tracing of their cell source during primitive hematopoiesis (Fig. 9, E and F). Furthermore, coimmunostaining for tdT and Ter-119 on E12.5 tissue sections showed that the majority of Ter-119⁺ definitive erythroid cells of the fetal liver were also labeled by tdT, indicating that 4OHT induction at E7.5 could label the transient definitive wave (Fig. S5, C and D). Since our findings had ruled out the possibility that the endocardium contained the HE, the *Cdh5-2A-CreER* could accurately capture the hematopoietic output of the endothelium of YS and AGM upon 4OHT treatment. Immunostaining for tdT and F4/80 on E16.5 heart sections also showed that >90% macrophages in different regions of the heart were labeled by tdT (Fig. 9, G and F).

To examine the origins of cardiac macrophages during EHT of definitive hematopoiesis, we treated reporter mice with 4OHT at E10.5 and performed analysis at E12.5 and E16.5 (Figs. 9 H and S5 E). Indeed, the microglia were no longer labeled by tdT (Figs. 9 I and S5 F). Furthermore, we did not detect any Ter-119⁺ tdT⁺ erythroid cells in E12.5 fetal liver, which is mostly generated from YS-derived primitive or transient definitive hematopoiesis (Soares-da-Silva et al., 2021), indicating that 4OHT treatment at E10.5 could no longer track transient hematopoiesis in our mouse model (Fig. S5, G and H). These data suggested that induction at E10.5 could specifically track AGM/HSC definitive hematopoiesis. Immunostaining for tdT and F4/80 on E16.5 heart sections showed that 10–20% of macrophages in different regions of the heart were tdT⁺, confirming their cellular origin during definitive hematopoiesis (Fig. 9, J and K). Collectively, our data suggest that cardiac-resident macrophages are mainly derived from EHT during YS-derived primitive/transient definitive hematopoiesis and AGM-derived definitive hematopoiesis (Fig. 9, L).

Discussion

In this study, we reexamined the origins of cardiac-resident macrophages in the developing heart. By using *Mef2c-AHF-Cre* and *Npr3-CreER* genetic tools, we revealed that Mef2c- and Npr3-derived endocardial cells minimally gave rise to cardiac macrophages and circulating blood cells, respectively. Furthermore, we generated the *Cdh5-2A-CreER* knock-in line to efficiently label endothelial cells of YS and AGM and demonstrated that cardiac macrophages of the developing heart were mostly derived from EHT during primitive and transient definitive hematopoiesis in the YS, with some being generated from definitive hematopoiesis in the AGM region.

DNA site-specific recombination systems have been widely used for lineage tracing and cell fate-mapping studies in vivo. Expression efficiency of the reporter gene depends on the recombination events mediated by Cre recombinase, which is driven under the control of a specific gene promoter. Therefore, the cell-specific nature of the promoter is essentially the linchpin of using this technology (Tian et al., 2015). If activation of the gene promoter is not operated in a cell-specific manner, the ectopic activity of the promoter in "unwanted" cell types will lead to discrepancies or even contradictory conclusions drawn from different studies (Liu et al., 2020). For instance, Nkx2.5⁺ cells are mainly regarded as cardiovascular progenitors that contribute to various cardiac lineages including myocytes and endocardial cells (Stanley et al., 2002). However, Nkx2.5-lineage⁺ cells also contribute to endothelial cells of YS and AGM, so the *Nkx2.5-Cre* line would not be a cell-specific tool for the evaluation of hemogenic potential of the endocardium (Stanley et al., 2002; Zamir et al., 2017). Similarly, we found that Nfatc1 was not specifically expressed by the endocardium. We used three different types of Nfatc1 knock-in lines (*Nfatc1-2A-CreER*, *Nfatc1-ires-Cre*, and *Nfatc1-2A-Dre*) to systematically analyze the cell fate of endothelium-derived cells throughout different regions of the embryos, including YS and AGM. Noticeably, >45 and 32% of endothelial cells of the YS and AGM, respectively, were labeled in the *Nfatc1-2A-CreER;R26-tdTomato* reporter mice, casting significant concern over the conclusion on the hemogenic potential of the endocardium based on fate mapping through Nfatc1. Furthermore, by RT-qPCR analysis and an inducible genetic labeling strategy, we found that a subset of cardiac-resident macrophages, circulating macrophages, and monocytes autonomously expressed the *Nfatc1* gene. Therefore, the macrophages and monocytes in the circulation and at various cardiac regions were directly labeled by *Nfatc1-ires-Cre* in addition to the HE of YS and DA.

During murine development, activation of gene expression is dynamic over time. Therefore, Cre-based tracing can mark target cells based on expression of a gene at one time that can also be expressed by nontarget cells at another time if the gene is not specifically activated in the target cells. Very often, we have yet to uncover a marker gene for a specific cell type. Therefore, the constitutively active Cre driver is not suitable for cell-specific fate-mapping studies, as it labels all cells that have historically expressed the nonspecific genes. Nevertheless, if the expression kinetics of a specific gene is known in the target cells, an inducible genetic labeling tool could sometimes be used to
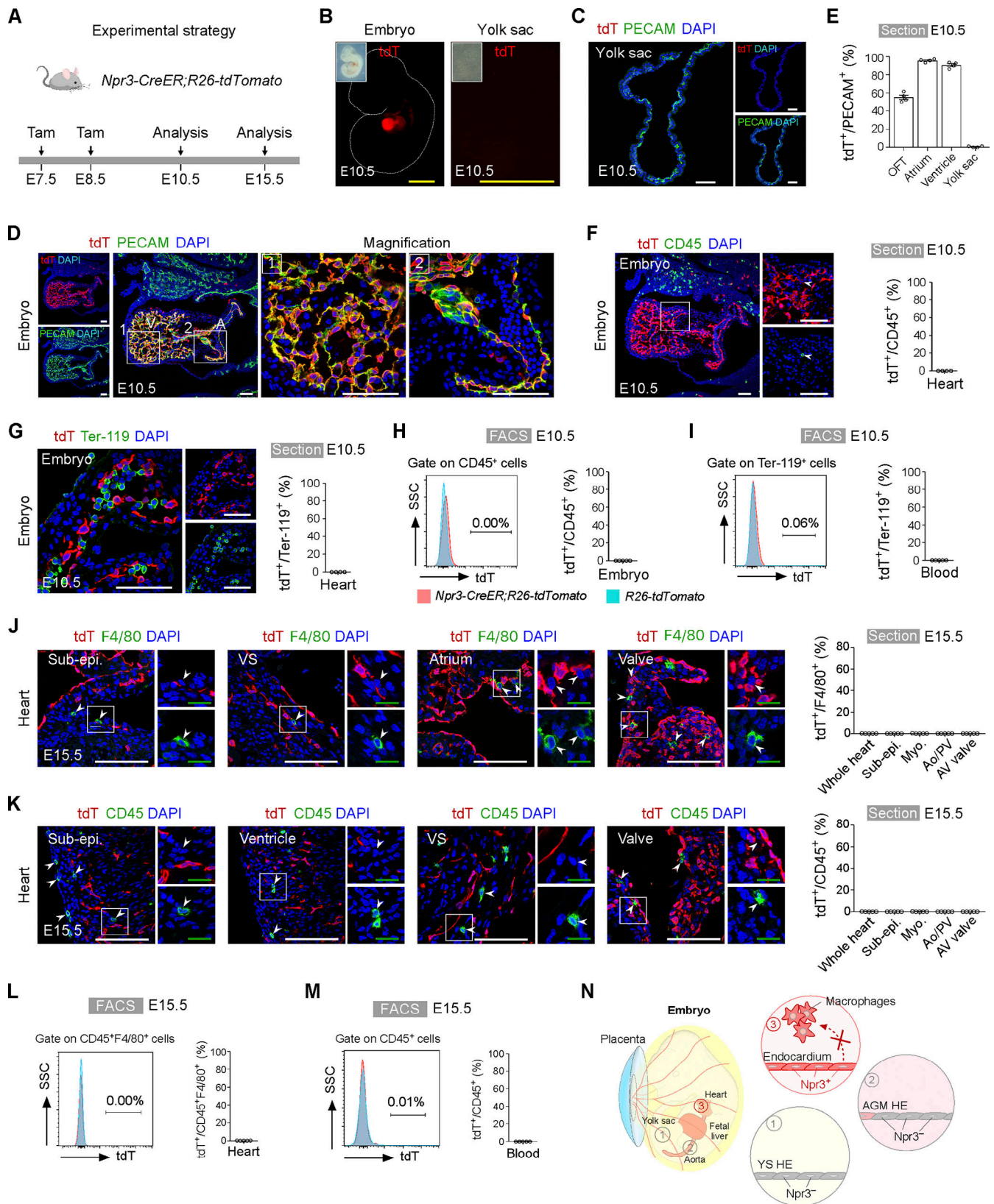
Figure 7. **Npr3-CreER–labeled endocardial cells contribute minimally to heart macrophages. (A)** Strategy for lineage tracing of Npr3^{+} endocardial cells using *Npr3-CreER;R26-tdTomato* mice. **(B)** Whole-mount fluorescence of E10.5 embryo and YS. **(C and D)** Immunostaining for tdT and PECAM on sections of E10.5 YS (C) and embryo (D). **(E)** Quantification of the percentage of PECAM^{+} endothelial cells expressing tdT in different regions. Data are presented as mean ± SEM; *n* = 4 mice per group. **(F)** Immunostaining for tdT and CD45 on E10.5 sections (left). White arrowheads, tdT^{-}CD45^{+} immune cells. Quantification of the percentage of CD45^{+} cells expressing tdT (right). Data are presented as mean ± SEM; *n* = 4 mice per group. **(G)** Immunostaining for tdT and Ter-119 on E10.5

sections (left). Quantification of the percentage of Ter-119^{+} cells expressing tdT (right). Data are presented as mean ± SEM; n = 4 mice per group. **(H)** Flow cytometric quantification of CD45^{+} immune cells of embryo expressing tdT. Data are presented as mean ± SEM; n = 5 mice per group. SSC, side scatter. **(I)** Flow cytometric quantification of Ter-119^{+} cells of embryo expressing tdT. Data are presented as mean ± SEM; n = 5 mice per group. **(J)** Immunostaining for tdT and F4/80 on E15.5 heart sections (left). White arrowheads, tdT[−]F4/80[+] macrophages. Quantification of the percentage of F4/80[+] macrophages expressing tdT (right). Data are presented as mean ± SEM; n = 5 mice per group. **(K)** Immunostaining for tdT and CD45 on E15.5 heart sections (left). White arrowheads, tdT^{−}CD45^{+} white blood cells. Quantification of the percentage of CD45^{+} blood cells expressing tdT (right). Data are presented as mean ± SEM; n = 5 mice per group. **(L and M)** Flow cytometric analysis of CD45^{+}F4/80^{+} macrophages of E15.5 heart (L) and CD45^{+} white blood cells of E15.5 blood (M) expressing tdT. Data are presented as mean ± SEM; n = 5 mice per group. **(N)** Cartoon image showing Npr3-labeled endocardial cells do not contribute to heart macrophages. A, atrium; Myo, myocardium; Sub-epi, subepicardium; Trab, trabeculae; V, ventricle; VS, ventricular septum. Scale bars, yellow, 1 mm; white, 100 µm; green, 20 µm.

---

minimize this deficiency. The inducible CreER driver could then temporally and spatially regulate the recombination of Cre-loxP, which could specifically target the cells of interest. In this study, we found that *Nfatc1-ires-Cre*–labeled cells contributed to ~50% of CD45^{+}F4/80^{+} cardiac macrophages of the E15.5 heart. Because of the nonspecific expression of the *Nfatc1* gene in multiple cell types, we summarized three possible sources of Nfatc1-labeled cardiac macrophages, including the hematopoietic output derived from Nfatc1-labeled HE of YS and DA; the Nfatc1^{+} cardiac macrophages directly labeled by *Nfatc1-ires-Cre*; and the circulating Nfatc1^{+} macrophages and monocytes labeled by *Nfatc1-ires-Cre*. The contributions of heart macrophages from these three Nfatc1 genetic tools are different, which are likely to come from the difference in recombination efficiency. The purpose of using all these Nfatc1 tools in our study is to demonstrate its broad expression in various tissues such as YS, AGM, and immune cells, in addition to endocardial cells.

Considering the nonspecific expression of Nfatc1 in multiple endothelial and white blood cell types, neither the constitutively active nor inducible Cre driven by *Nfatc1* should be used for accurately labeling endocardial-derived cells. We further conducted ex vivo hematopoietic colony-forming assays that showed no hematopoietic activity of the Nfatc1^{+} endocardium. On the other hand, we used alternative strategies to label endocardial cells and to distinguish them from endothelial cells of the HE of YS and AGM. *Mef2c* is a specific gene marker of the second heart field progenitors that contribute to the myocardium and endocardium (Verzi et al., 2005). Using *Mef2c-AHF-Cre;R26-tdTomato* reporter mice, we found that *Mef2c-Cre* labeled the majority of endocardial cells of the OFT and atrium, but minimally labeled cardiac macrophages or circulating blood cells. The same results were confirmed using another endocardial Cre driver, *Npr3-CreER*, that could efficiently label endocardial cells and distinguish them from endothelial cells of YS. The inducible drivers are limited by incomplete recombination, so it is still possible that the lineage-negative endocardial cells were hemogenic, as the *Npr3-CreER* did not label all endocardial cells, and the *Npr3-CreER* randomly labeled the vast majority of endocardial cells (>90%) in this study. Therefore, these fate-mapping data may raise great concern about data interpretation regarding the concept of hemogenic endocardium in previous studies (Grainger and Traver, 2019; Nakano et al., 2013; Shigeta et al., 2019; Zamir et al., 2017). However, in our ex vivo hematopoietic colony-forming assays, we isolated the whole-heart tissues that were unable to contribute to any macrophage colony. Therefore, the possibility that the lineage-negative endocardium was hemogenic seemed unlikely.
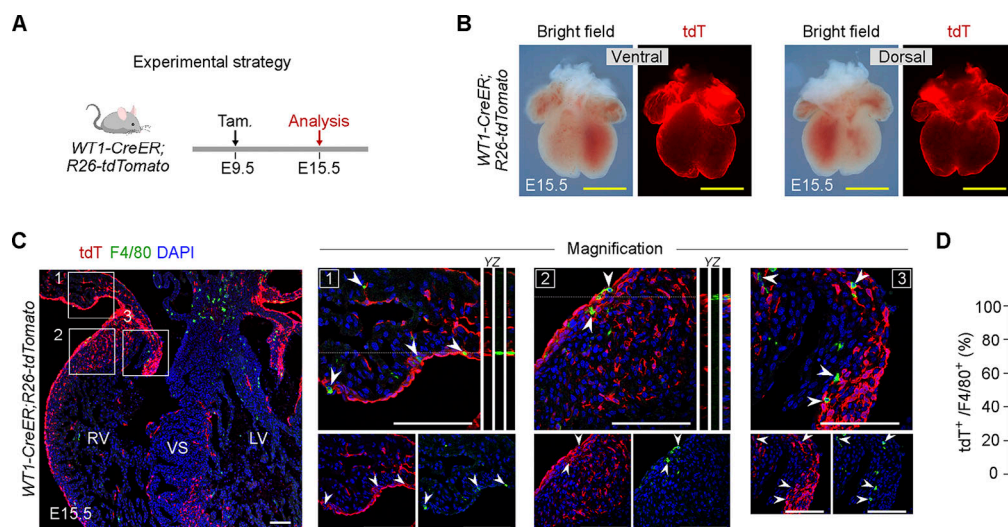
Figure 8. Epicardial cells do not contribute to cardiac macrophages. (A) Strategy for lineage tracing of WT1^{+} epicardial cells using *Wt1-CreER;R26-tdTomato* mice. **(B)** Whole-mount fluorescence of the E15.5 heart. **(C)** Immunostaining for tdT and F4/80 on E15.5 heart section showing that Wt1^{+} epicardial cells do not contribute to macrophages (arrowheads). **(D)** Quantification of the percentage of tdT[+]F4/80[+] macrophages. Data are presented as mean ± SEM; n = 4 mice per group. LV, left ventricle; RV, right ventricle; VS, ventricular septum. Scale bars, yellow, 1 mm; white, 100 µm.
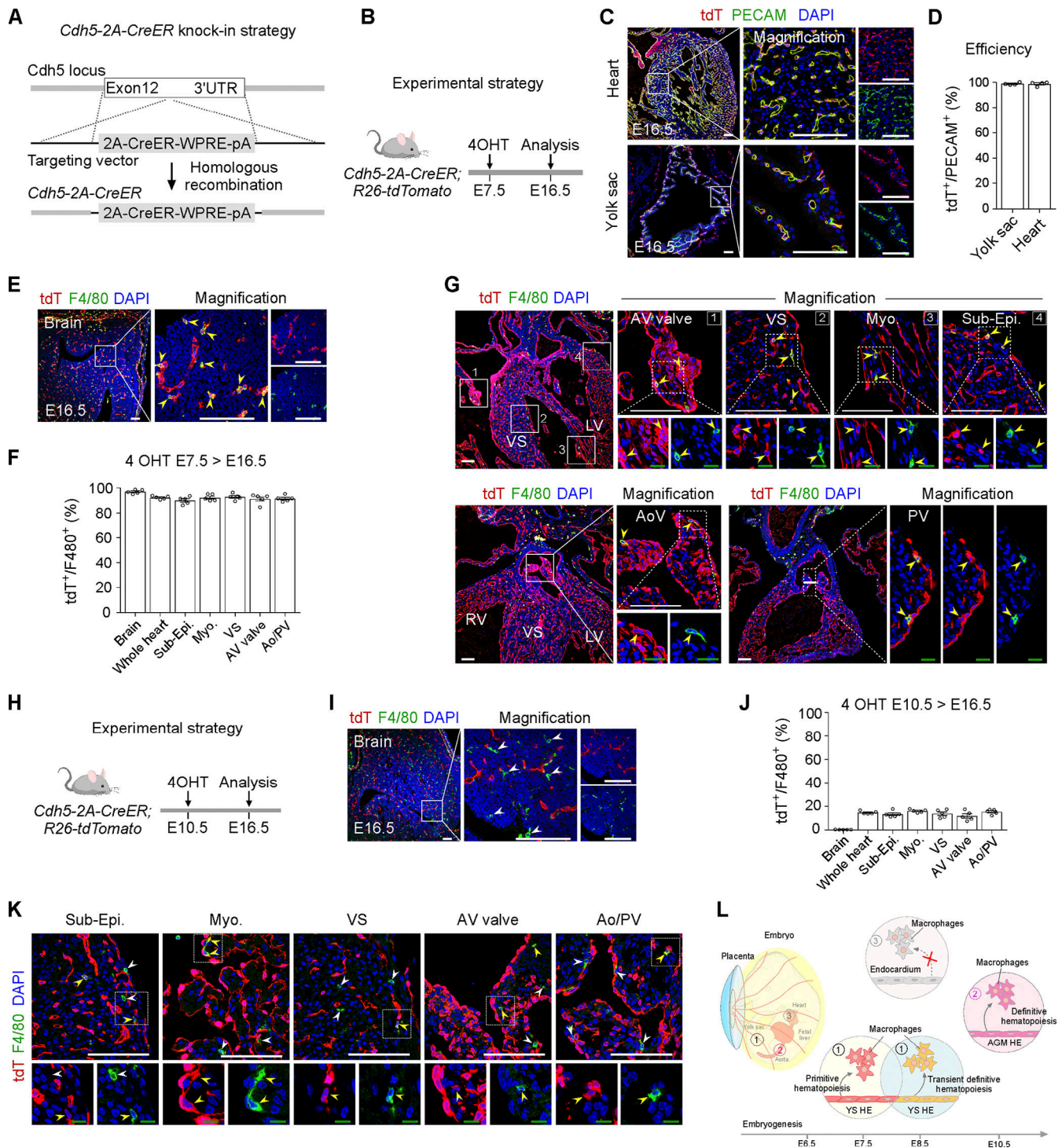
Figure 9. **Primitive and transient definitive hematopoiesis of the YS and definitive hematopoiesis of the AGM contribute to heart macrophages. (A)** A schematic diagram showing knock-in strategy of *Cdh5-2A-CreER* line by homologous recombination. **(B)** Schematic showing the experimental strategy. **(C)** Immunostaining for tdT and PECAM on E16.5 heart and YS of *Cdh5-2A-CreER;R26-tdTomato* mice. **(D)** Quantification of the percentage of PECAM+ endothelial cells expressing tdT. Data are presented as mean ± SEM; n = 4 mice per group. **(E)** Immunostaining for tdT and F4/80 on E16.5 brain sections. Yellow arrowheads, tdT+F4/80+ microglia. **(F)** Quantification of the percentage of F4/80+ macrophages expressing tdT in E16.5 brain and heart. Data are presented as mean ± SEM; n = 5 mice per group. **(G)** Immunostaining for tdT and F4/80 on E16.5 heart sections. Yellow arrowheads, tdT+F4/80+ macrophages. **(H)** Schematic showing the experimental strategy. **(I)** Immunostaining for tdT and F4/80 on E16.5 brain section. White arrowheads, tdT−F4/80+ microglia. **(J)** Quantification of the percentage of F4/80+ macrophages expressing tdT in E16.5 brain and heart. Data are presented as mean ± SEM; n = 5 mice per group. **(K)** Immunostaining for tdT and F4/80 on heart sections. Yellow arrowheads, tdT+F4/80+ macrophages; white arrowheads, tdT−F4/80+ macrophages. **(L)** Cartoon image showing that primitive and transient definitive hematopoiesis of YS HE and definitive hematopoiesis of AGM HE, but not endocardium, contribute to cardiac macrophages. LV, left ventricle; RV, right ventricle; Myo, Myocardium; Sub-epi, subepicardium; Trab, trabeculae; VS, ventricular septum. White bars, 100 μm. Green bars, 20 μm.

To further understand the origins of cardiac macrophages, and whether endothelial cells of YS and AGM were the major cell sources of these cells in the developing heart, we performed lineage tracing through an endothelial Cre driver. We generated a new *Cdh5-2A-CreER* knock-in line with high efficiency, as >98% of endothelial cells in YS and AGM were labeled after Tam treatment. It is acknowledged that endothelial cells contribute to the three distinct waves of hematopoiesis during embryogenesis (Ginhoux and Guilliams, 2016; Gomez Perdiguero et al., 2015; Hoeffel et al., 2015; Shalaby et al., 1997). Through temporally labeling endothelial cells by 4OHT administration at E7.5 or E10.5, we selectively captured the hematopoietic output of the HE of YS and AGM, respectively, during primitive and definitive hematopoiesis in *Cdh5-2A-CreER;R26-tdTomato* reporter mice. Fate-mapping data clearly showed that cardiac macrophages had three distinct origins: mostly from the primitive/transient definitive waves, and some from definitive hematopoiesis. Indeed, our data were also consistent with previous reports (Epelman et al., 2014a; Epelman et al., 2014b; Gomez Perdiguero et al., 2015; Hoeffel et al., 2015; Gentek, 2018).

Collectively, by using more specific genetic tools that distinguished endocardial cells from endothelial cells of YS and AGM, we demonstrated that the endocardium was not hemogenic and did not give rise to cardiac macrophages or other circulating blood cells. The macrophages that have been reported as essential for valvular remodeling (Grainger and Traver, 2019; Kim et al., 2021; Shigeta et al., 2019) were more likely derived from the *Nfatc1-Cre*–labeled endothelial cells of YS or AGM. How these cardiac macrophages are recruited from the circulation and adopt new functions in the developing heart merits further investigation. Essentially, elucidating the developmental origins of cardiac macrophages and their functional roles in the developing heart will advance our understanding of cardiac development, pathogenesis, and regeneration.

Materials and methods
Mice
All mouse experiments were carried out strictly in accordance with the guidelines of the Institutional Animal Care and Use Committee of the State Key Laboratory of Cell Biology, Shanghai Institute of Biochemistry and Cell Biology, Center for Excellence in Molecular Cell Science, University of Chinese Academy of Sciences, Chinese Academy of Sciences. *R26-tdTomato, R26-rox-tdTomato, Nfatc1-ires-Cre, Nfatc1-2A-Dre, Nfatc1-2A-CreER, Npr3-CreER, Mef2c-AHF-Cre,* and *Wt1-CreER* mouse lines were described previously (De Val et al., 2004; Zhang et al., 2017; Zhang et al., 2016a; Zhang et al., 2016b; Zhou et al., 2008). The *Npr3-ZsGreen* knock-in mouse line was generated by knocking ZsGreen before exon 1 of *Npr3* gene (after 5′ UTR). The *Cdh5-2A-CreER* knock-in mouse line was generated by knocking 2A-CreER after exon 12 of Cdh5 gene (before 3′ UTR). The *Npr3-ZsGreen* and *Cdh5-2A-CreER* lines were generated by Shanghai Model Organisms Center. All mice used for experiments were kept at C57BL6 background or C57BL6/ICR mixed background. Both male and female mice were randomly used in this study. The blinding experiments were not used in this study. Tam (Sigma-Aldrich; T5648) was dissolved in corn oil and stored at 4°C. Tamoxifen treatment to mice at

the indicated time points was given by oral gavage (0.2 mg/g). 4OHT was dissolved in absolute ethanol and stored at 4°C. 4OHT was treated in each mouse by oral gavage (0.1 mg/g).

Genomic PCR
Genomic DNA was extracted from the mouse tail. Briefly, the tail tissues were collected and then lysed at 55°C overnight, followed by centrifugation of the mixture at 20,000 rpm for 8 min. The supernatant containing the genomic DNA was obtained. Next, we used isopropanol to precipitate the DNA that was further washed in 70% ethanol followed by centrifugation for 5 min. DNase/RNase-free water was used to dissolve the DNA.

Tissue collection and immunofluorescent staining
Briefly, after euthanizing the pregnant mice, the embryos or heart tissues were fixed in 4% PFA (P6148; Sigma-Aldrich) at 4°C for 30–60 min according to the tissue size. After several washes in PBS, whole-mount bright-field and fluorescence images were acquired on a Zeiss stereoscope (Axio Zoom.V16). The tissues were dehydrated in 30% sucrose overnight at 4°C and allowed to sink, and then embedded in optimal cutting temperature solution (Sakura) before freezing at –80°C. 9–10-μm frozen sections were collected on slides and stored at –20°C. For immunofluorescent staining, the slides were first put in a fume hood for air dry, followed by washing in PBS to remove optimal cutting temperature solution. Slides were blocked in 5% PBSST (0.1% Triton X-100 and 5% donkey serum in PBS) for 30 min, followed by incubation with primary antibodies overnight at 4°C in the dark. Primary antibodies used in this study: F4/80 (rat, ab6640; 1:500 dilution; Abcam), CD68 (rat, MCA1957; 1:400 dilution; Bio-Rad), ZsGreen (rabbit, 632474; 1:1,000 dilution; Clontech), tdT (rabbit, 600-401-379; 1:1,000 dilution; Rockland), VE-cad (goat, AF1002; 1:100 dilution; R&D), ERG (rabbit, ab92513; 1:400 dilution; Abcam), CD45 (rat, 17-0451-82; 1:100 dilution; eBioscience), Ter-119 (rat, 14-5921-85, 1:400 dilution; eBioscience), CD31 (rat, 553370, 1:500 dilution; BD Pharmingen), Runx1 (rabbit, ab92336, 1:200 dilution; Abcam). Plvap (rat, 5353849, 1:300; BD Pharmingen). On the following day, the slides were washed in PBS for 15 min to remove primary antibodies and then incubated with secondary antibodies for 40 min at room temperature in the dark. After washing in PBS for 15 min for removing secondary antibodies, the slides were mounted with DAPI-containing mounting medium and stored in –20°C. Alexa fluorescence conjugated secondary antibodies were used to develop signals. HRP-conjugated antibodies were sometimes used to amplify the weak signals. Secondary antibodies used in this study: Alexa donkey anti-rabbit 555 (donkey, A31572, 1:1,000; Invitrogen), donkey anti-rat 647 (donkey, ab150155, 1:1,000; Abcam), donkey anti-goat 647 (donkey, A21447, 1:1,000; Invitrogen), Immpress goat anti-rat (goat, MP-7444, 1:3; Vector Laboratories). Fluorescence images were acquired by Olympus confocal microscopy system (FV1200). ImageJ (National Institutes of Health) software was used to analyze the images.

Single cell isolation and flow cytometry
The embryonic tissue collection method
The embryonic macrophages and endothelial cells were isolated by collagenase-based method. Briefly, the embryonic tissues

were collected at the indicated time points and cut into small pieces, followed by digestion in 4 ml lysis buffer containing 2 mg/ml collagenase type I (17100-017; Thermo Fisher Scientific) and 0.1 mg/ml DNase I (LS002139-100MG; Worthington) in PBS at 37°C for 40 min. The mixture was pipetted up and down every 15 min to ensure a full lysis. After digestion, the mixture was added in 4 ml PBS and subsequently passed through 40-mm cell strainers (352340; BD Falcon). The cells were centrifuged at 1,000 g at 4°C for 5 min. The cell pellets were lysed in 1 ml RBC lysis buffer (00-4333-57; eBioscience) at room temperature for 3 min, followed by washing in 10 ml PBS. After centrifugation at 1,000 g at 4°C for 5 min, the pellets were resuspended in PBS and then stained with fluorescence-conjugated primary antibodies at 4°C for 30 min.

The peripheral blood collection method

To collect fetal peripheral blood, embryos were washed to get rid of maternal blood. After that, the embryo was decapitated in an anticoagulant tube (367841; BD) containing 4 ml PBS and 5 µl DNase I (0.1 mg/ml, LS002139-100MG; Worthington). The blood cells were transferred to a 15-ml centrifuge tube and centrifuged at 1,000 g at 4°C for 5 min. The supernatant was discarded. For analysis of red blood cells, no RBC lysis buffer was used, and the sample was directly resuspended in PBS and stained with fluorescence-conjugated primary antibodies at 4°C for 30 min. For other analysis, red blood cell lysis was carried out by adding 1 ml of RBC lysis buffer (00-4333-57; eBioscience) at room temperature for 5 min, followed by resuspension in 10 ml PBS and centrifugation at 1,000 g at 4°C for 5 min. After that, the samples were resuspended in PBS and stained with fluorescence conjugated primary antibodies at 4°C for 30 min.

The staining protocol

Primary antibodies used in this study: F4/80 PE-Cy7 (rat, 123114, 1:200; BioLegend), CD45 FITC (rat, 11-0451, 1:200; eBioscience), CD11b PE-Cy7 (rat, 25-0112-82, 1:200; eBioscience), CD45 APC (rat, 47-0451, 1:200; eBioscience), CD45 APC-eFluor 780 (rat, 47-0451-82, 1:200; eBioscience), Ly6G APC (17-9668-80, rat, 1:200; eBioscience), CD11b APC (rat, 17-0112-81, 1:200; eBioscience), CD3 FITC (rat, 11-0032-82, 1:200; eBioscience), and CD19 APC-eFluor 780 (rat, 47-0193-80, 1:200; eBioscience). After that, the cells were washed and resuspended in PBS, followed by staining in DAPI (Vector Laboratories) at 4°C for 5 min to exclude dead cells. Live cell analysis was performed by Beckman Coulter CytoFLEX S, Thermo Attune NxT, FACSAria SORP, and BD FACSAria Fusion. The FACS data were analyzed with the FlowJo software.

RNA extraction and RT-qPCR assay

The cells were isolated in centrifuge tubes (MCT-150-C; Axygen) by FACSAria SORP, or BD FACSAria Fusion. The total RNA of the cells was then isolated by using Trizol reagent (15596018; Invitrogen). 1 ml Trizol reagent was added to each sample tube and incubated at room temperature for 5 min. The samples were centrifuged at 20,000 rpm at 4°C for 5 min. The supernatant of samples was transferred into a new 1.5-ml tube and supplemented with 200 µl chloroform. The samples were then vortexed for 20 s and left at room temperature for 15 min, followed by centrifugation at 20,000 rpm at 4°C for 15 min, and the

supernatant was transferred into a new 1.5 ml tube. 200 µl isopropyl alcohol was then added into each tube with mixing, followed by resting at room temperature for 10 min. Next, the samples were centrifuged at 20,000 rpm at 4°C for 15 min and the RNA was washed with 75% EtOH. RNase/DNase-free water (10977023; Invitrogen) was used for dissolving the RNA. The RNA was converted to cDNA by using the PrimeScript RT reagent Kit with gDNA Eraser (RR047A; TaKaRa). SYBR Green PCR Master Mix (4367659; Thermo Fisher Scientific) was used to amplify cDNA in ABI Step-one real-time PCR system (Applied Biosystems). Primers used: Nfatc1: forward, 5′-GAGGAACACGCTGATGCC-3′; reverse, 5′-AGGCGAGTTGGGTTGGAT-3′. GAPDH: forward, 5′-TTGTCTCCT GCGACTTCAAC-3′; reverse, 5′-GTCATACCAGGAAATGAGCTTG-3′.

Hematopoietic colony-forming assays

Hematopoietic colony-forming assay was designed to assess the hematopoietic potential and was performed according to the protocols described by Nakano et al. (2013). Briefly, the embryonic tissues including YS, caudal half, head, and heart regions were dissected and precultured on OP9 stromal cells for 4 d at 37°C in 24-well plates containing 1 ml α-MEM (Gibco) containing 20% fetal bovine serum (Gibco) and 1% penicillin/ streptomycin supplemented with stem cell factor (50 ng/ml), thrombopoietin (5 ng/ml), IL-3 (IL-3, 5 ng/ml), IL-6 (IL-6, 5 ng/ ml), and Flt-3 ligand (Flt-3L, 10 ng/ml). After 4 d, the tissues were transferred from 24-well plates into 1.5 ml tubes and dissociated mechanically by pipetting, and the stromal cells were removed through filtering. The cells were then transferred into methylcellulose supplemented with IL-3, IL-6, stem cell factor, and erythropoietin (MethoCult GF M3434; Stem Cell Technologies) in 1:10 ratio, followed by mixing well and plating with 400 µl medium at the bottom of the 24-well plates. The cells were cultured at 37°C for 10 d. The hematopoietic colonies were analyzed with microscope (ECHO/RVL-100-G) according to the manufacturer's instruction.

Fluorescence microscopy

Whole-mount bright-field and epifluorescence imaging was performed at room temperature with a Zeiss stereoscope (Axio Zoom.V16) equipped with a camera (AxioCam HRM). Images were acquired with a 16× objective (PlanApo Z, NA: 0.25) using Zen software. Confocal microcopy analysis was performed at room temperature with an Olympus FV1200. Confocal images were taken with 10× (UPLSAPO, NA: 0.4) and 60× (UPLSAPO, NA: 1.3) objectives using FLUOVIEW software. The imaging medium of 10× objective is air and the 60× is silicone oil. The images were analyzed by ImageJ (National Institutes of Health).

Statistical analysis

The normality of all samples was tested by using Shapiro-Wilk test. All data were presented as mean values ± SEM of biological replicates acquired from at least three independent experiments as indicated in figure legends.

Online supplemental material

Fig. S1 shows the contribution of Nfatc1^{+} cells to heart macrophages and circulating blood cells. Fig. S2 shows that Nfatc1^{+}

endocardium contributes to heart macrophages. Fig. S3 shows that Mef2c-AHF-Cre–labeled endocardium does not contribute to heart macrophages or circulating blood cells. Fig. S4 shows that Npr3-CreER–labeled endocardial cells do not contribute to heart macrophages and circulating blood cells. Fig. S5 shows that *Cdh5-2A-CreER* is able to label the primitive and transient definitive hematopoiesis of YS HE and definitive hematopoiesis of AGM HE under different Tam treatment, respectively.

Data availability

This study includes no data deposited in external repositories. All materials are available from the corresponding author upon reasonable request and without undue delay.

Acknowledgments

References

Abu-Issa, R., and M.L. Kirby. 2007. Heart field: From mesoderm to heart tube. *Annu. Rev. Cell Dev. Biol.* 23:45–68. https://doi.org/10.1146/annurev.cellbio.23.090506.123331

Aurora, A.B., E.R. Porrello, W. Tan, A.I. Mahmoud, J.A. Hill, R. Bassel-Duby, H.A. Sadek, and E.N. Olson. 2014. Macrophages are required for neonatal heart regeneration. *J. Clin. Invest.* 124:1382–1392. https://doi.org/10.1172/jci72181

Boisset, J.C., W. van Cappellen, C. Andrieu-Soler, N. Galjart, E. Dzierzak, and C. Robin. 2010. In vivo imaging of haematopoietic cells emerging from the mouse aortic endothelium. *Nature.* 464:116–120. https://doi.org/10.1038/nature08764

Chen, Q., H. Zhang, Y. Liu, S. Adams, H. Eilken, M. Stehling, M. Corada, E. Dejana, B. Zhou, and R.H. Adams. 2016. Endothelial cells are progenitors of cardiac pericytes and vascular smooth muscle cells. *Nat. Commun.* 7: 12422. https://doi.org/10.1038/ncomms12422

de Lange, F.J., A.F. Moorman, R.H. Anderson, J. Manner, A.T. Soufan, C. de Gier-de Vries, M.D. Schneider, S. Webb, M.J. van den Hoff, and V.M. Christoffels. 2004. Lineage and morphogenetic analysis of the cardiac valves. *Circ. Res.* 95: 645–654. https://doi.org/10.1161/01.RES.0000141429.13560.cb

De Val, S., J.P. Anderson, A.B. Heldt, D. Khiem, S.M. Xu, and B.L. Black. 2004. Mef2c is activated directly by Ets transcription factors through an evolutionarily conserved endothelial cell-specific enhancer. *Dev. Biol.* 275:424–434. https://doi.org/10.1016/j.ydbio.2004.08.016

DeRuiter, M.C., R.E. Poelmann, I. Vanderplasdevries, M.M.T. Mentink, and A.C. Gittenbergerdegroot. 1992. The development of the myocardium and endocardium in mouse embryos: Fusion of 2 heart tubes. *Anat. Embryol.* 185:461–473. https://doi.org/10.1007/BF00174084

Dzierzak, E., and N.A. Speck. 2008. Of lineage and legacy: The development of mammalian hematopoietic stem cells. *Nat. Immunol.* 9:129–136. https://doi.org/10.1038/ni1560

Epelman, S., K.J. Lavine, A.E. Beaudin, D.K. Sojka, J.A. Carrero, B. Calderon, T. Brija, E.L. Gautier, S. Ivanov, A.T. Satpathy, et al. 2014a. Embryonic and adult-derived resident cardiac macrophages are maintained through distinct mechanisms at steady state and during inflammation. *Immunity.* 40:91–104. https://doi.org/10.1016/j.immuni.2013.11.019

Epelman, S., K.J. Lavine, and G.J. Randolph. 2014b. Origin and functions of tissue macrophages. *Immunity.* 41:21–35. https://doi.org/10.1016/j.immuni.2014.06.013

Gentek, R., C. Ghigo, G. Hoeffel, M.J. Bulle, R. Msallam, G. Gautier, P. Launay, J. Chen, F. Ginhoux, and M. Bajénoff. 2018. Hemogenic endothelial fate mapping reveals dual developmental origin of mast cells. *Immunity.* 48: 1160–1171.e5. https://doi.org/10.1016/j.immuni.2018.04.025

Ginhoux, F., and M. Guilliams. 2016. Tissue-resident macrophage ontogeny and homeostasis. *Immunity.* 44:439–449. https://doi.org/10.1016/j.immuni.2016.02.024

Ginhoux, F., M. Greter, M. Leboeuf, S. Nandi, P. See, S. Gokhan, M.F. Mehler, S.J. Conway, L.G. Ng, E.R. Stanley, et al. 2010. Fate mapping analysis reveals that adult microglia derive from primitive macrophages. *Science.* 330:841–845. https://doi.org/10.1126/science.1194637

Gomez Perdiguero, E., K. Klapproth, C. Schulz, K. Busch, E. Azzoni, L. Crozet, H. Garner, C. Trouillet, M.F. de Bruijn, F. Geissmann, and H.R. Rode-wald. 2015. Tissue-resident macrophages originate from yolk-sac-derived erythro-myeloid progenitors. *Nature.* 518:547–551. https://doi.org/10.1038/nature13989

Grainger, S., and D. Traver. 2019. Embryonic immune cells remodel the heart. *Dev. Cell.* 48:595–596. https://doi.org/10.1016/j.devcel.2019.02.017

He, L., Y. Li, Y. Li, W. Pu, X. Huang, X. Tian, Y. Wang, H. Zhang, Q. Liu, L. Zhang, et al. 2017. Enhancing the precision of genetic lineage tracing using dual recombinases. *Nat. Med.* 23:1488–1498. https://doi.org/10.1038/nm.4437

Hoeffel, G., J. Chen, Y. Lavin, D. Low, F.F. Almeida, P. See, A.E. Beaudin, J. Lum, I. Low, E.C. Forsberg, et al. 2015. C-Myb⁺ erythro-myeloid progenitor-derived fetal monocytes give rise to adult tissue-resident macrophages. *Immunity.* 42:665–678. https://doi.org/10.1016/j.immuni.2015.03.011

Hulsmans, M., S. Clauss, L. Xiao, A.D. Aguirre, K.R. King, A. Hanley, W.J. Hucker, E.M. Wulfers, G. Seemann, G. Courties, et al. 2017. Macrophages facilitate electrical conduction in the heart. *Cell.* 169:510–522.e20. https://doi.org/10.1016/j.cell.2017.03.050

Ji, R.P., C.K.L. Phoon, O. Aristizabal, K.E. McGrath, J. Palis, and D.H. Turnbull. 2003. Onset of cardiac function during early mouse embryogenesis coincides with entry of primitive erythroblasts into the embryo proper. *Circ. Res.* 92:133–135. https://doi.org/10.1161/01.res.0000056532.18710.c0

Kim, A.J., N. Xu, and K.E. Yutzey. 2021. Macrophage lineages in heart valve development and disease. *Cardiovasc. Res.* 117:663–673. https://doi.org/10.1093/cvr/cvaa062

Lavine, K.J., S. Epelman, K. Uchida, K.J. Weber, C.G. Nichols, J.D. Schilling, D.M. Ornitz, G.J. Randolph, and D.L. Mann. 2014. Distinct macrophage lineages contribute to disparate patterns of cardiac recovery and re-modeling in the neonatal and adult heart. *Proc. Natl. Acad. Sci. USA.* 111: 16029–16034. https://doi.org/10.1073/pnas.1406508111

Leid, J., J. Carrelha, H. Boukarabila, S. Epelman, S.E. Jacobsen, and K.J. Lavine. 2016. Primitive embryonic macrophages are required for coronary development and maturation. *Circ. Res.* 118:1498–1511. https://doi.org/10.1161/CIRCRESAHA.115.308270

Liu, K., W. Yu, M. Tang, J. Tang, X. Liu, Q. Liu, Y. Li, L. He, L. Zhang, S.M. Evans, et al. 2018. A dual genetic tracing system identifies diverse and dynamic origins of cardiac valve mesenchyme. *Development.* 145: dev167775. https://doi.org/10.1242/dev.167775

Liu, K., H. Jin, and B. Zhou. 2020. Genetic lineage tracing with multiple DNA recombinases: A user's guide for conducting more precise cell fate mapping studies. *J. Biol. Chem.* 295:6413–6424. https://doi.org/10.1074/jbc.REV120.011631

Lorchner, H., J. Poling, P. Gajawada, Y. Hou, V. Polyakova, S. Kostin, J.M. Adrian-Segarra, T. Boettger, A. Wietelmann, H. Warnecke, et al. 2015. Myocardial healing requires Reg3β-dependent accumulation of macrophages in the ischemic heart. *Nat. Med.* 21:353–362. https://doi.org/10.1038/nm.3816

Medvinsky, A., and E. Dzierzak. 1996. Definitive hematopoiesis is autonomously initiated by the AGM region. *Cell.* 86:897–906. https://doi.org/10.1016/s0092-8674(00)80165-8

Nahrendorf, M., F.K. Swirski, E. Aikawa, L. Stangenberg, T. Wurdinger, J.L. Figueiredo, P. Libby, R. Weissleder, and M.J. Pittet. 2007. The healing myocardium sequentially mobilizes two monocyte subsets with divergent and complementary functions. *J. Exp. Med.* 204:3037–3047. https://doi.org/10.1084/jem.20070885

Nakano, H., X. Liu, A. Arshi, Y. Nakashima, B. van Handel, R. Sasidharan, A.W. Harmon, J.H. Shin, R.J. Schwartz, S.J. Conway, et al. 2013. Haemogenic endocardium contributes to transient definitive haematopoiesis. *Nat. Commun.* 4:1564. https://doi.org/10.1038/ncomms2569

North, T.E., M.F. de Bruijn, T. Stacy, L. Talebian, E. Lind, C. Robin, M. Binder, E. Dzierzak, and N.A. Speck. 2002. Runx1 expression marks long-term repopulating hematopoietic stem cells in the midgestation mouse embryo. *Immunity.* 16:661–672. https://doi.org/10.1016/s1074-7613(02)00296-0

Shalaby, F., J. Ho, W.L. Stanford, K.D. Fischer, A.C. Schuh, L. Schwartz, A. Bernstein, and J. Rossant. 1997. A requirement for Flk1 in primitive and definitive hematopoiesis and vasculogenesis. *Cell.* 89:981–990. https://doi.org/10.1016/s0092-8674(00)80283-4

Shigeta, A., V. Huang, J. Zuo, R. Besada, Y. Nakashima, Y. Lu, Y. Ding, M. Pellegrini, R.P. Kulkarni, T. Hsiai, et al. 2019. Endocardially derived macrophages are essential for valvular remodeling. *Dev. Cell.* 48: 617–630.e3. https://doi.org/10.1016/j.devcel.2019.01.021

Soares-da-Silva, F., L. Freyer, R. Elsaid, O. Burlen-Defranoux, L. Iturri, O. Sismeiro, O.P. Pinto-do, E. Gomez-Perdiguero, and A. Cumano. 2021. Yolk sac, but not hematopoietic stem cell-derived progenitors, sustain erythropoiesis throughout murine embryonic life. *J. Exp. Med.* 218: e20201729. https://doi.org/10.1084/jem.20201729

Stanley, E.G., C. Biben, A. Elefanty, L. Barnett, F. Koentgen, L. Robb, and R.P. Harvey. 2002. Efficient cre-mediated deletion in cardiac progenitor cells conferred by a 3′ UTR-ires-Cre allele of the homeobox gene Nkx2-5. *Int. J. Dev. Biol.* 46:431–439

Tian, X., W.T. Pu, and B. Zhou. 2015. Cellular origin and developmental program of coronary angiogenesis. *Circ. Res.* 116:515–530. https://doi.org/10.1161/CIRCRESAHA.116.305097

Verzi, M.P., D.J. McCulley, S. De Val, E. Dodou, and B.L. Black. 2005. The right ventricle, outflow tract, and ventricular septum comprise a restricted expression domain within the secondary/anterior heart field. *Dev. Biol.* 287:134–145. https://doi.org/10.1016/j.ydbio.2005.08.041

Wu, B., Z. Zhang, W. Lui, X. Chen, Y. Wang, A.A. Chamberlain, R.A. Moreno-Rodriguez, R.R. Markwald, B.P. O'Rourke, D.J. Sharp, et al. 2012. Endocardial cells form the coronary arteries by angiogenesis through myocardial-endocardial VEGF signaling. *Cell.* 151:1083–1096. https://doi.org/10.1016/j.cell.2012.10.023

Zamir, L., R. Singh, E. Nathan, R. Patrick, O. Yifa, Y. Yahalom-Ronen, A.A. Arraf, T.M. Schultheiss, S. Suo, J.J. Han, et al. 2017. Nkx2.5 marks angioblasts that contribute to hemogenic endothelium of the endocardium and dorsal aorta. *Elife.* 6:e20994. https://doi.org/10.7554/elife.20994

Zhang, H., W. Pu, G. Li, X. Huang, L. He, X. Tian, Q. Liu, L. Zhang, S.M. Wu, H.M. Sucov, and B. Zhou. 2016a. Endocardium minimally contributes to coronary endothelium in the embryonic ventricular free walls. *Circ. Res.* 118:1880–1893. https://doi.org/10.1161/CIRCRESAHA.116.308749

Zhang, H., W. Pu, Q. Liu, L. He, X. Huang, X. Tian, L. Zhang, Y. Nie, S. Hu, K.O. Lui, and B. Zhou. 2016b. Endocardium contributes to cardiac fat. *Circ. Res.* 118:254–265. https://doi.org/10.1161/CIRCRESAHA.115.307202

Zhang, H., X. Huang, K. Liu, J. Tang, L. He, W. Pu, Q. Liu, Y. Li, X. Tian, Y. Wang, et al. 2017. Fibroblasts in an endocardial fibroelastosis disease model mainly originate from mesenchymal derivatives of epicardium. *Cell Res.* 27:1157–1177. https://doi.org/10.1038/cr.2017.103

Zhou, B., R.Q. Cron, B. Wu, A. Genin, Z. Wang, S. Liu, P. Robson, and H.S. Baldwin. 2002. Regulation of the murine Nfatc1 gene by NFATc2. *J. Biol. Chem.* 277:10704–10711. https://doi.org/10.1074/jbc.m107068200

Zhou, B., Q. Ma, S. Rajagopal, S.M. Wu, I. Domian, J. Rivera-Feliciano, D. Jiang, A. von Gise, S. Ikeda, K.R. Chien, and W.T. Pu. 2008. Epicardial progenitors contribute to the cardiomyocyte lineage in the developing heart. *Nature.* 454:109–113. https://doi.org/10.1038/nature07060
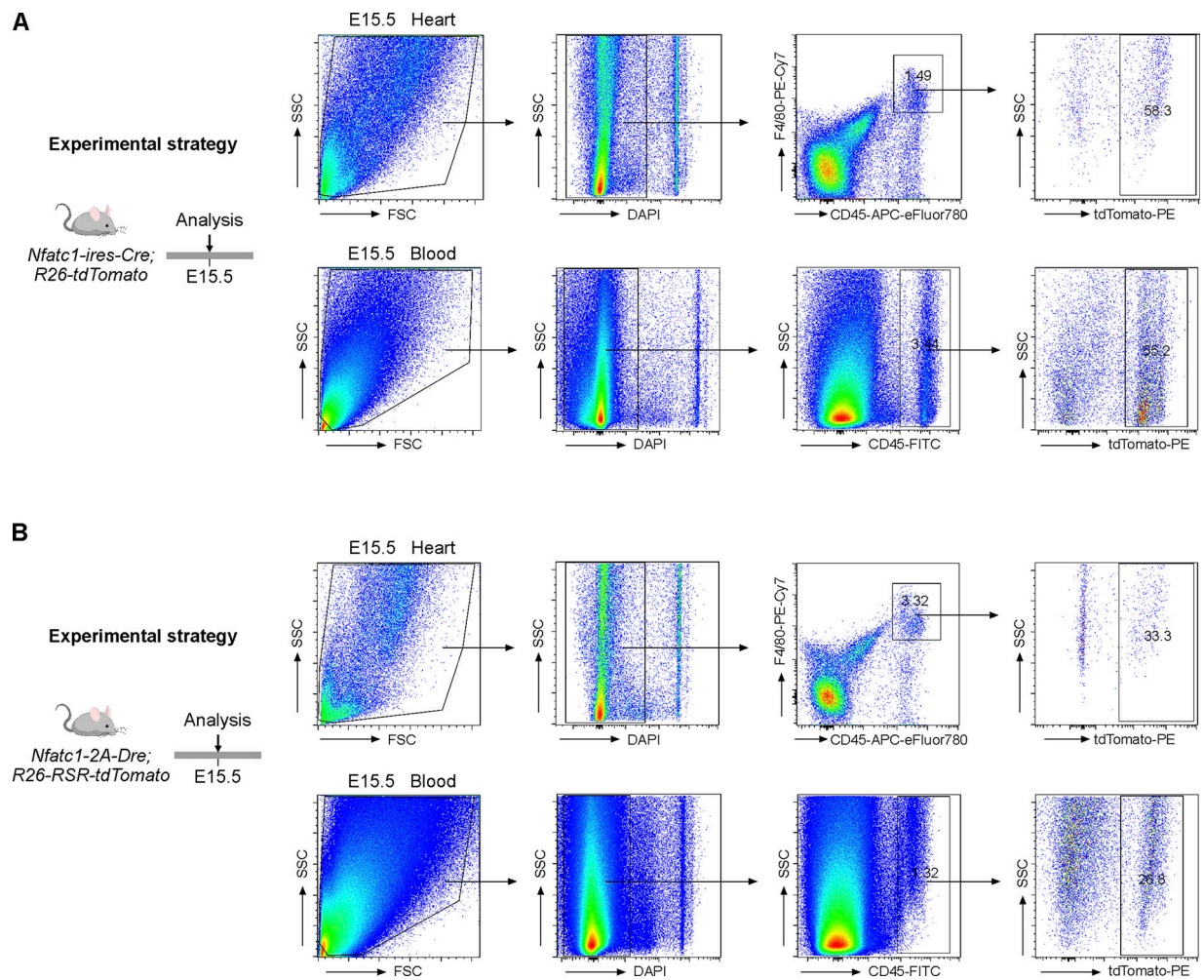
Figure S1.   **Nfatc1+ cells contribute to heart macrophages and circulating blood cells.** Related to Fig. 2. **(A)** FACS analysis of the percentage of CD45+F4/80+ heart macrophages and CD45+ blood cells expressing tdT of E15.5 *Nfatc1-ires-Cre;R26-tdTomato* mice. FSC, forward scatter; SSC, side scatter. **(B)** FACS analysis of the percentage of CD45+F4/80+ heart macrophages and CD45+ blood cells expressing tdT of E15.5 *Nfatc1-2A-Dre;R26-RSR-tdTomato* mice. *n* = 5 mice per group.
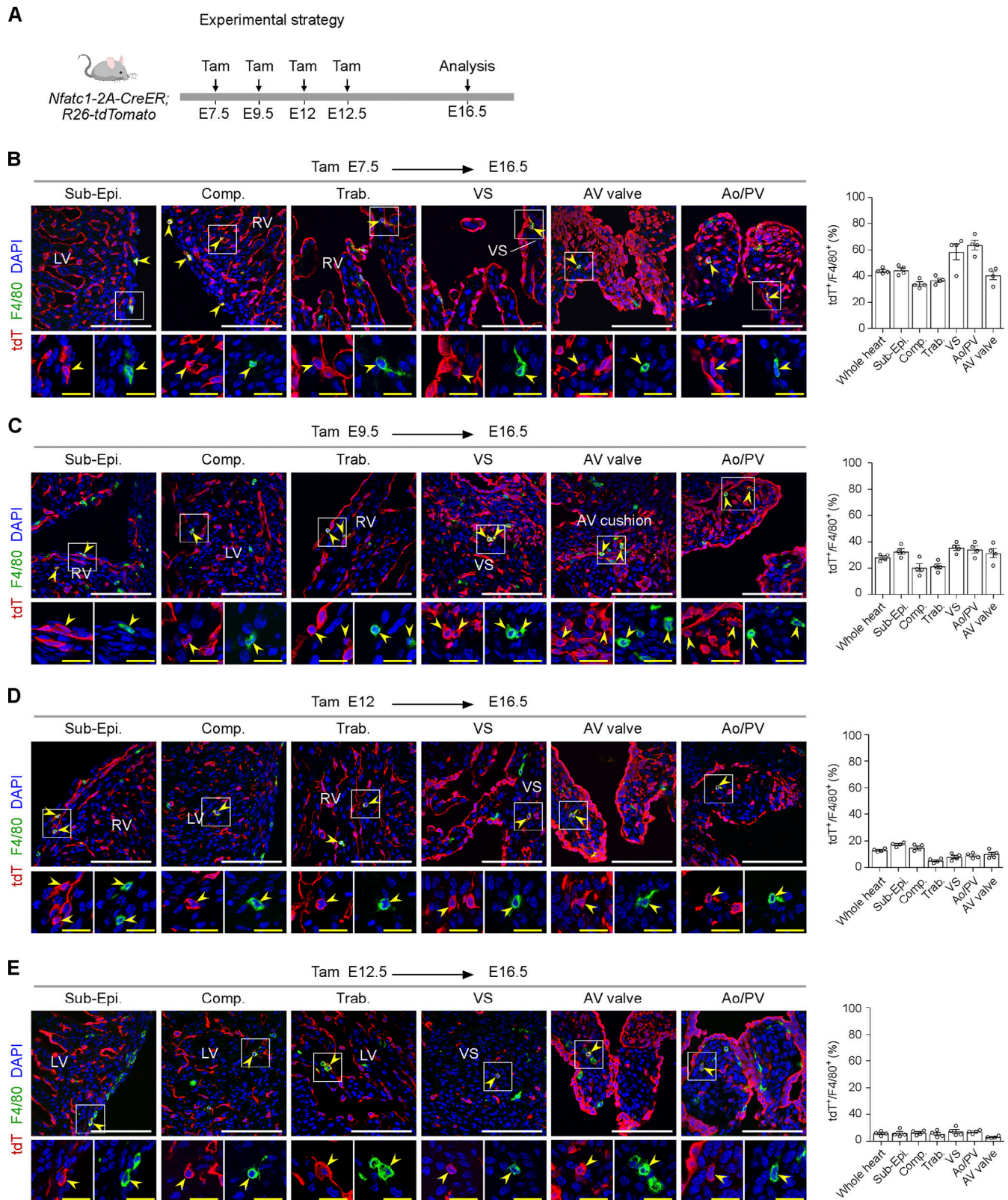
Figure S2. **Nfatc1+ endothelium contributes to heart macrophages.** Related to Fig. 2. **(A)** Strategy for lineage tracing of Nfatc1+ cells using *Nfatc1-2A-CreER;R26-tdTomato* mice. Tam is administered at E7.5, E9.5, E12, or E12.5 for labeling Nfatc1+ cells, and the hearts are analyzed at E16.5. **(B–E)** Immunostaining for tdT and F4/80 on E16.5 heart sections after Tam treatment at E7.5 (B), E9.5 (C), E12 (D), or E12.5 (E). Yellow arrowheads, tdT+F4/80+ macrophages. Quantification of the percentage of tdT+F4/80+ macrophages are in the adjacent right panels. Data are presented as mean ± SEM; *n* = 4 mice per group. Comp, Compaction; LV, left ventricle; RV, right ventricle; Sub-Epi, subepicardium; Trab, trabeculae; VS, ventricular septum. Scale bars, white,100 µm; yellow, 20 µm.
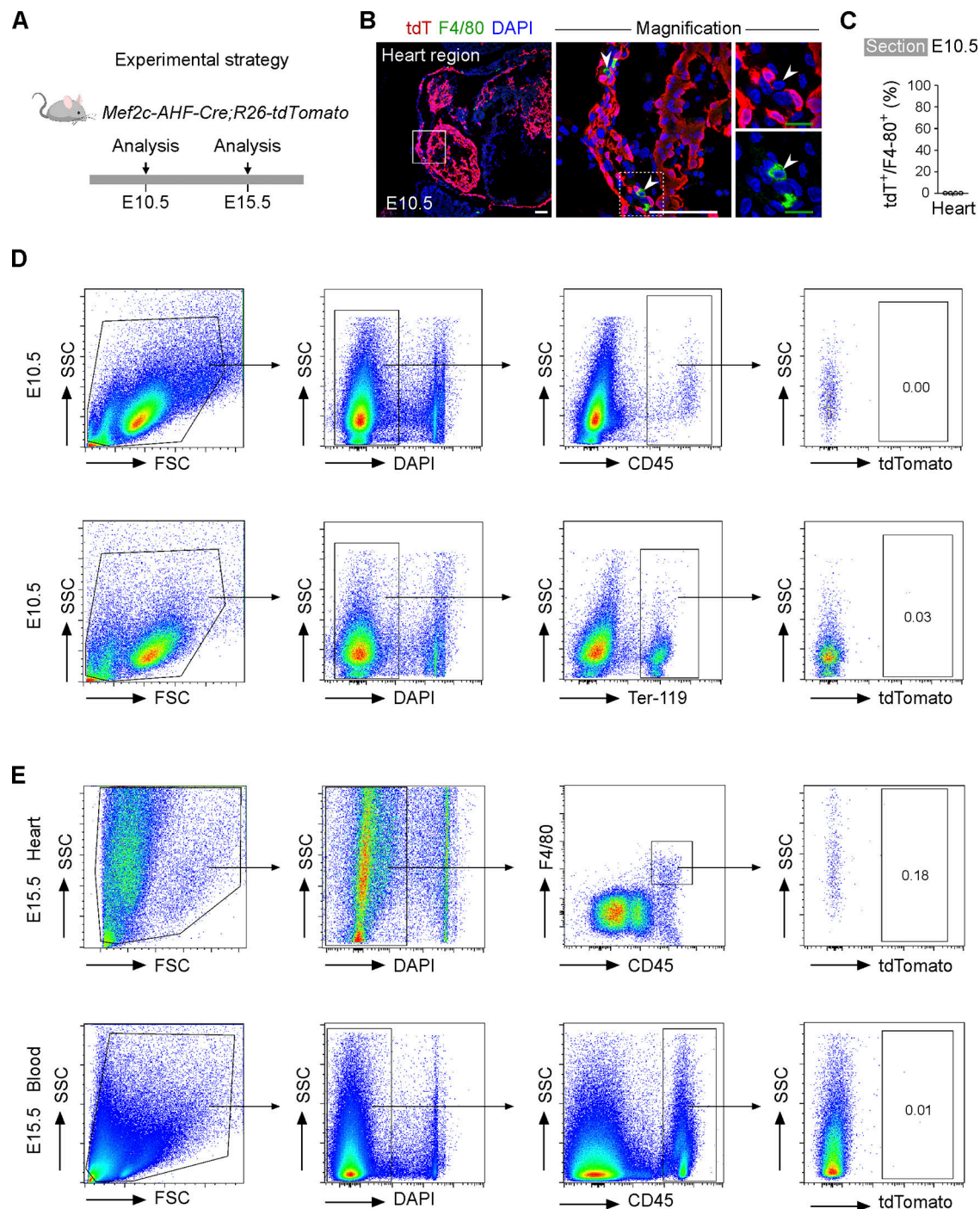
Figure S3. **Mef2c-AHF-Cre–labeled endocardium contributes minimally to heart macrophages or circulating blood cells.** Related to Fig. 6. **(A)** Strategy for lineage tracing of Mef2c-derived endocardium by using *Mef2c-AHF-Cre;R26-tdTomato* mice. **(B)** Immunostaining for tdT and F4/80 on sections of E10.5 embryo. White arrowheads, tdT⁻F4/80⁺ heart macrophages. **(C)** Quantification of the percentage of F4/80⁺ macrophages expressing tdT. Data are presented as mean ± SEM; *n* = 4 mice per group. **(D)** FACS analysis of the percentage of CD45⁺ immune cells of whole embryo and Ter-119⁺ circulating erythrocytes expressing tdT of E10.5 *Mef2c-AHF-Cre;R26-tdTomato* mice. *n* = 5 mice per group. FSC, forward scatter; SSC, side scatter. **(E)** FACS analysis of the percentage of CD45⁺F4/80⁺ heart macrophages and CD45⁺ circulating blood cells expressing tdT of E15.5 *Mef2c-AHF-Cre;R26-tdTomato* mice. *n* = 5 mice per group. Scale bars, white, 100 µm; green, 20 µm.

Liu et al.
Cellular origin of cardiac macrophages

Journal of Cell Biology S3
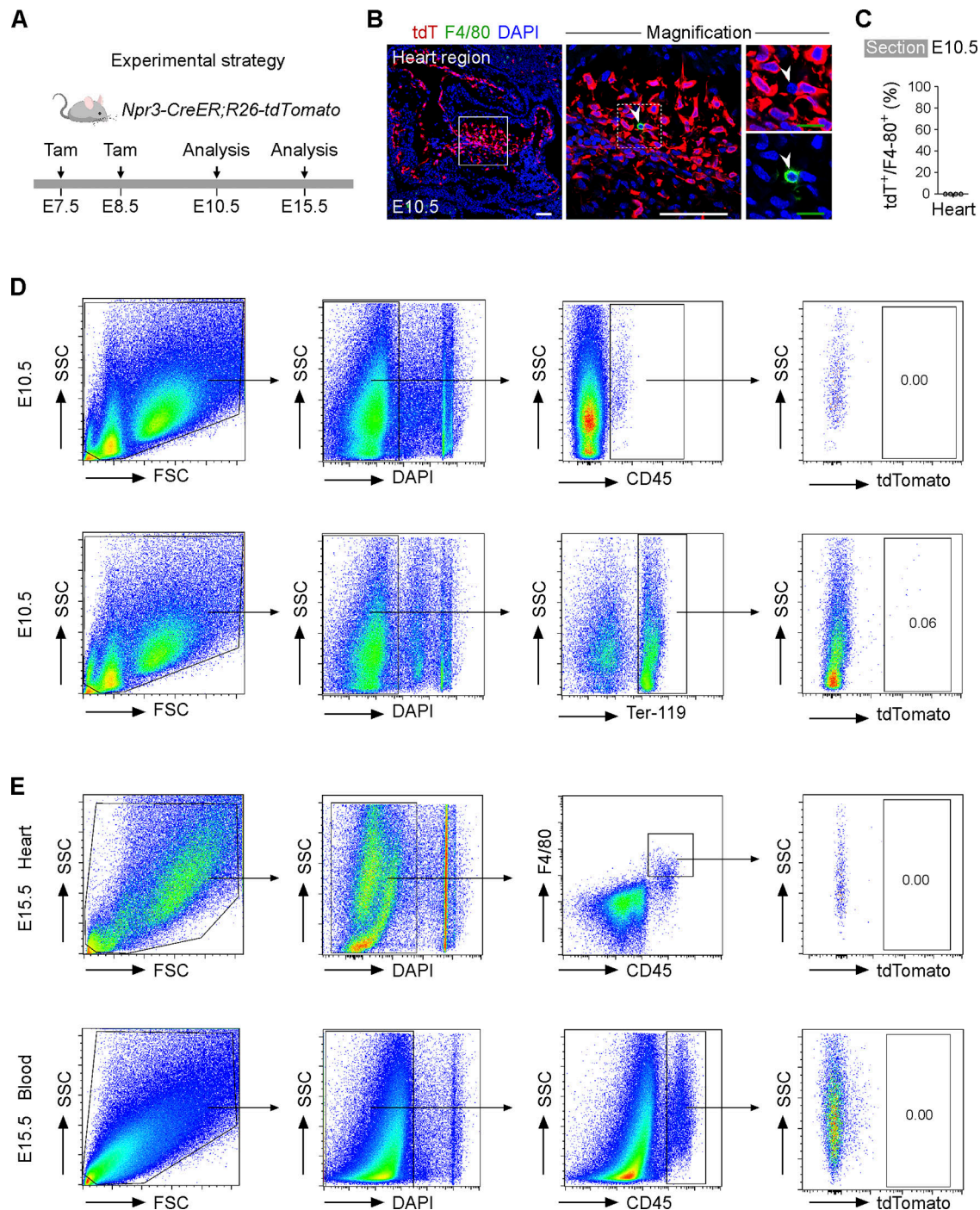https://doi.org/10.1083/jcb.202108093

Figure S4. ***Npr3-CreER*–labeled endocardial cells contribute minimally to heart macrophages and circulating blood cells.** Related to Fig. 7. **(A)** Strategy for lineage tracing of Npr3+ endocardium by using *Npr3-CreER;R26-tdTomato* mice. **(B)** Immunostaining for tdT and F4/80 on sections of E10.5 embryo. White arrowheads, tdT⁻F4/80⁺ heart macrophages. **(C)** Quantification of the percentage of F4/80⁺ macrophages expressing tdT. Data are presented as mean ± SEM; *n* = 4 mice per group. **(D)** FACS analysis of the percentage of CD45⁺ immune cells of whole embryo and Ter-119⁺ circulating erythrocytes expressing tdT of E10.5 *Npr3-CreER;R26-tdTomato* mice. *n* = 5 mice per group. FSC, forward scatter; SSC, side scatter. **(E)** FACS analysis of the percentage of CD45⁺F4/80⁺ heart macrophages and CD45⁺ circulating blood cells expressing tdT of E15.5 *Npr3-CreER;R26-tdTomato* mice. *n* = 5 mice per group. Scale bars, white, 100 µm; green, 20 µm.
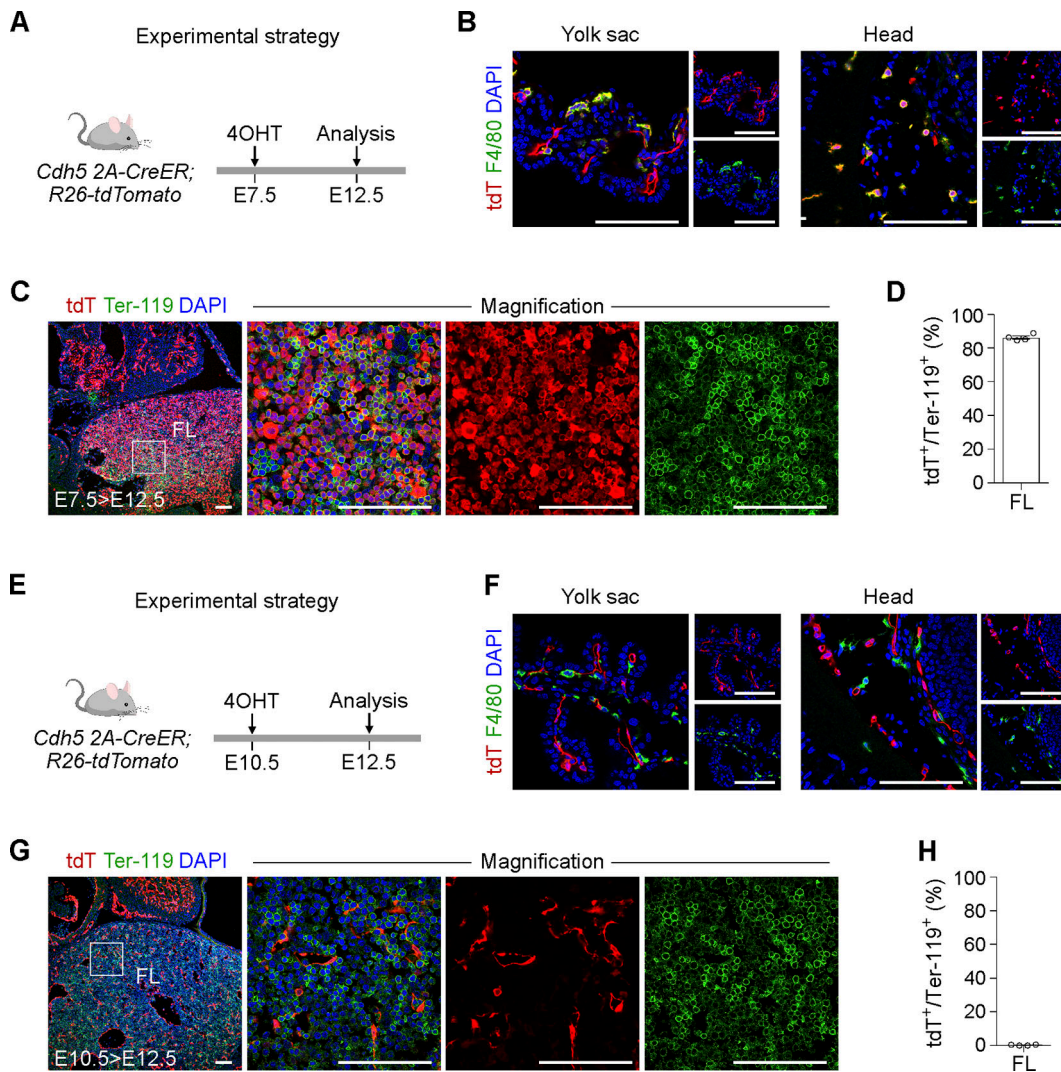
Figure S5. **Cdh5-2A-CreER is able to label the primitive and transient definitive hematopoiesis of YS HE and definitive hematopoiesis of AGM HE under different Tam treatment strategies.** Related to Fig. 9. **(A)** Schematic showing the experimental design. **(B)** Immunostaining for tdT and F4/80 on YS and head sections of the embryo. **(C)** Immunostaining for tdT and Ter-119 on sections of E12.5 embryo. **(D)** Quantification of the percentage of Ter-119+ erythrocytes expressing tdT. **(E)** Schematic figure showing the experimental design. **(F)** Immunostaining for tdT and F4/80 on sections of E12.5 embryo. **(G)** Immunostaining for tdT and Ter-119 on sections of E12.5 embryo. **(H)** Quantification of the percentage of Ter-119+ erythrocytes expressing tdT. Data are presented as mean ± SEM; n = 4 mice per group. FL, Fetal liver. Scale bars, 100 μm.